

# Finite difference methods for fractional Laplacians

Yanghong Huang<sup>\*1</sup> and Adam Oberman<sup>†2</sup>

<sup>1</sup>School of Mathematics, The University of Manchester, Manchester, M13 9PL, UK

<sup>2</sup>Department of Mathematics and Statistics, McGill University, Montreal, QC H3A 0B9, Canada

May 11, 2019

## Abstract

The fractional Laplacian  $(-\Delta)^{\alpha/2}$  is the prototypical non-local elliptic operator. While analytical theory has been advanced and understood for some time, there remain many open problems in the numerical analysis of the operator. In this article, we study several different finite difference discretisations of the fractional Laplacian on uniform grids in one dimension that takes the same form. Many properties can be compared and summarised in this relatively simple setting, to tackle more important questions like the nonlocality, singularity and flat tails common in practical implementations. The accuracy and the asymptotic behaviours of the methods are also studied, together with treatment of the far field boundary conditions, providing a unified perspective on the further development of the scheme in higher dimensions.

## Contents

<b>1</b>	<b>Introduction</b>	<b>2</b>
<b>2</b>	<b>Semi-discrete Fourier analysis and spectral representation</b>	<b>4</b>
2.1	Background on semi-discrete Fourier analysis . . . . .	5
2.2	Spectral representation of the schemes (FLh) . . . . .	6
<b>3</b>	<b>Discrete identities and inequalities</b>	<b>7</b>

---

\*yanghong.huang@manchester.ac.uk

†adam.oberman@mcgill.ca

<b>4</b>	<b>Presentation of the weights</b>	<b>9</b>
4.1	Spectral weights and sinc interpolation . . . . .	10
4.2	Weights from regularized Fourier symbol . . . . .	13
4.3	Gorenflo-Mainardi scheme using Grünwald-Letnikov weights . . . . .	14
4.4	The finite difference-quadrature method . . . . .	15
<b>5</b>	<b>Discussions and Comparisons of the weights</b>	<b>16</b>
5.1	Basic properties of the weights . . . . .	16
5.2	Order of accuracy via the rescaled symbols . . . . .	18
5.3	Summary on the properties of the schemes . . . . .	20
<b>6</b>	<b>Truncation of the far-field boundary conditions</b>	<b>21</b>
<b>7</b>	<b>Convergence for equations with fractional Laplacian operators</b>	<b>24</b>
<b>8</b>	<b>Numerical experiments and applications to nonlinear PDEs</b>	<b>26</b>
8.1	Accuracy when the solutions are non-smooth . . . . .	26
8.2	The extended Dirichlet problem . . . . .	27
8.3	Fractional heat equation . . . . .	28
8.4	Fractal Burgers Equation . . . . .	29
8.5	Fractional thin film equation . . . . .	32
<b>9</b>	<b>Conclusions</b>	<b>32</b>

# 1 Introduction

Anomalous diffusion is a phenomenon of current interest, occurring in various physical systems [25] as well as in financial modelling [39, 55, 40]. In this article, we focus on the numerical approximations of the fractional Laplacian, the prototypical nonlocal operator intimately related to anomalous diffusion. In the whole space  $\mathbb{R}^n$ , the fractional Laplacian of order  $\alpha \in (0, 2)$  can be defined in several equivalent ways [35, 48, 53]. Two of the most common ones are given by the Fourier transform

$$\mathcal{F}[(-\Delta)^{\alpha/2}u](\xi) = |\xi|^\alpha \mathcal{F}[u](\xi). \tag{1}$$

and by the singular integral

$$(-\Delta)^{\alpha/2}u(x) = C_{n,\alpha} \int_{\mathbb{R}^n} \frac{u(x) - u(y)}{|x - y|^{n+\alpha}} dy, \tag{2}$$

where the constant coefficient  $C_{n,\alpha}$  is given by

$$C_{n,\alpha} = \frac{\alpha 2^{\alpha-1} \Gamma\left(\frac{\alpha+n}{2}\right)}{\pi^{n/2} \Gamma\left(\frac{2-\alpha}{2}\right)}, \tag{3}$$

and  $\Gamma(t) = \int_0^\infty s^{t-1} e^{-s} ds$  is the Gamma function. Using the symmetric combination of two one-sided fractional derivatives [41, 43, 44, 45], the Fractional Laplacian in one dimension can be written as

$$(-\Delta)^{\alpha/2} u(x) = \frac{-\infty D_x^\alpha u(x) + {}_x D_\infty^\alpha u(x)}{2 \cos(\alpha\pi/2)}, \quad \alpha \neq 1. \quad (4)$$

Based on tools from functional calculus, the fractional Laplacian (more generally the fractional power of positive operators) can be represented as

$$(-\Delta)^{\alpha/2} u = \frac{1}{\Gamma(-\frac{\alpha}{2})} \int_0^\infty (e^{s\Delta} u - u) s^{-1-\alpha/2} ds. \quad (5)$$

Over the past decade, many important theoretical results of differential equations with the fractional Laplacian are established by building upon the definition using  $\alpha$ -harmonic extension proposed by Caffarelli and Silvestre [9].

All the previous definitions are equivalent in the whole space [34], at least when the operator is applied to proper classes of functions that decay fast enough at infinity. However, on bounded domains there are many non-equivalent definitions, according to the particular boundary conditions used. For this reason, the focus of the finite difference methods here is on the whole space, allowing a unified treatment of viewing many existing schemes and deriving new schemes. However, boundary conditions remain an important consideration, and will be touched on in later sections.

The fractional Laplacian can be evaluated numerically in various ways according to the equivalent definitions above, for instance, using either the spectral definition in Fourier space or the singular integral representation. A vast majority of existing schemes are based on fractional derivatives [38, 50], using variants of the classical Grünwald-Letnikov derivative [16, 43]. When used in the discretisation of fractional diffusion equations, the resulting schemes can usually be interpreted as a random walk with long range jumps [23, 22]. Another popular class of schemes use spectral decomposition in Fourier or other basis [8], usually only valid for finite spatial domains. In recent years, more numerical schemes are proposed, based on either the singular integral [18, 27], the one from functional calculus [10] and the harmonic extension [15, 42].

Despite the abundance of existing numerical methods to choose from, the presence of nonlocality, singularity as well as prevalent flat tails in the far field remains a challenging problem. In this paper, we provide a unified framework for the finite difference approximation of the fractional Laplacian. In one dimension, let  $u = \{u_j\}_{j \in \mathbb{Z}}$  be a function defined on the uniform grid  $\mathbb{Z}_h = \{jh \mid j \in \mathbb{Z}\}$  with spacing  $h > 0$ . The discrete operator, denoted as  $(-\Delta_h)^{\alpha/2}$ , evaluated at  $x_j = jh$  is given by

$$(-\Delta_h)^{\alpha/2} u_j = \sum_{k=-\infty}^{\infty} (u_j - u_{j-k}) w_k, \quad (\text{FLh})$$

with some prescribed weights  $\{w_k\}_{k \in \mathbb{Z}}$ . This special form of the scheme clearly resembles the singular integral (2) and is shown to be a multiplier in the appropriate spectral space below. This scheme already appeared several times explicitly or implicitly in the literature [6, 11, 18,

27], including the simplest choice  $w_k = C|k|^{-\alpha-1}$  ( $k \neq 0$ ) from [53]. However, its systematic study will be performed here for the first time, linking different definitions in the continuous setting and motivating new development in the future.

A few reasonable constraints on the weights  $w_k$  can be readily imposed without worrying about their exact values. Since the fractional Laplacian is symmetric under reflection, it is natural to require that  $w_k = w_{-k}$ . When the scheme (FLh) is used in the discretisation of the simplest fractional heat equation  $u_t + (-\Delta)^{\alpha/2}u = 0$  for the probability density  $u$ , the explicit Euler scheme  $(u_j^{n+1} - u_j^n)/\Delta t = (-\Delta_h)^{\alpha/2}u_j^n$  for  $u_j^{n+1}$  at time  $t_{n+1} = (n+1)\Delta t$  and space  $x_j = jh$  can be written as

$$u_j^{n+1} = (1 + \Delta t w_0)u_j^n + \sum_{k \neq 0} \Delta t w_k u_{j-k}^n. \quad (6)$$

The associated random walk interpretation as performed in [23, 22] suggests that the transition probability  $\Delta t w_k$  is non-negative, or the weights  $w_k$  with  $k \neq 0$  are non-negative. We will show that basic properties like symmetry and non-negativity of the weights are valid for almost all schemes discussed later, and are essential for other related properties like discrete maximum principle.

The analysis and numerical experiments with the scheme (FLh) performed in this paper is organised as follows. The semi-discrete Fourier Transform will be introduced next, revealing the relationship between the weights in (FLh) and the symbol in the spectral space, followed by some identities and inequalities in Section 3. Different weights are either derived or reviewed in Section 4, and their properties are summarised and compared in Section 5. Other issues about the treatment of far field boundary conditions and the convergence of the scheme for equations with the fractional Laplacian operator are discussed in Section 6 and Section 7. Finally we end with this paper with several numerical experiments in Section 8 and some final remarks on the extension into higher dimensions.

## 2 Semi-discrete Fourier analysis and spectral representation

Since  $(-\Delta)^{\alpha/2}$  is a pseudo-differential operator with symbol  $|\xi|^\alpha$ , its numerical discretisation is also expected to have a symbol (if it exists in an appropriate spectral space) that approximates  $|\xi|^\alpha$ . We show that *semi-discrete Fourier transform*, already well-known in the numerical analysis community [51], is the right tool to analyse the discrete scheme (FLh). The one-to-one correspondence between the weights  $w_k$  and the associated symbol will be established: the symbol is defined as a discrete sum involving the weights, and the weights can be calculated as a Fourier integral of the symbol. Moreover, explicit symbols are obtained for many popular schemes from the literature, including the spectrally accurate scheme with the exact symbol  $|\xi|^\alpha$ . To facilitate the discussion below, we introduce some function spaces

on the grid  $\mathbb{Z}_h = \{hk \mid k \in \mathbb{Z}\}$  and on the interval  $I_h = [-\pi/h, \pi/h]$ ,

$$\ell^2(\mathbb{Z}_h) = \left\{ v : \mathbb{Z}_h \rightarrow \mathbb{R} \mid h \sum_{j=-\infty}^{\infty} |v_j|^2 < \infty \right\},$$

$$L^2(I_h) = \left\{ \hat{v} : I_h \rightarrow \mathbb{R} \mid \int_{-\pi/h}^{\pi/h} |\hat{v}(\xi)|^2 d\xi < \infty \right\}.$$

Both  $\ell^2(\mathbb{Z}_h)$  and  $L^2(I_h)$  are Hilbert spaces, endowed with the inner products

$$\langle u, v \rangle_{\ell^2(\mathbb{Z}_h)} = h \sum_{j=-\infty}^{\infty} u_j \overline{v_j} \quad \text{and} \quad \langle \hat{u}, \hat{v} \rangle_{L^2(I_h)} = \int_{-\pi/h}^{\pi/h} \hat{u}(\xi) \overline{\hat{v}(\xi)} d\xi. \quad (7)$$

## 2.1 Background on semi-discrete Fourier analysis

Semi-discrete Fourier transform is intimately connected to the widely used Fourier transform and Fourier series, and can be motivated from the Fourier transform

$$\hat{v}(\xi) = \int_{-\infty}^{\infty} e^{-i\xi x} v(x) dx. \quad (8)$$

If the function  $v$  is defined on the grid  $\mathbb{Z}_h$  of our interest here, the natural modification of (8) is to replace the integral by its Trapezoidal rule

$$\hat{v}(\xi) = \mathcal{F}[v](\xi) = h \sum_{j=-\infty}^{\infty} e^{-i\xi x_j} v_j, \quad (9)$$

which is taken as the definition of our *semi-discrete Fourier Transform*. As a result, the transformed function  $\hat{v}(\xi)$  is periodic with period  $2\pi/h$  and it is more convenient to restrict the spectral space to be the interval  $I_h = [-\pi/h, \pi/h]$  instead of the real line  $\mathbb{R}$ . The Fourier transform (8) can be recovered from (9) in the limit as  $h$  goes to zero, and more detailed exposition about these transforms can be found in [51, Chapter 2].

Once the semi-discrete Fourier Transform (9) is defined, its inverse transform can also be readily worked out and takes the form

$$v_j = \mathcal{F}^{-1}[\hat{v}](x_j) = \frac{1}{2\pi} \int_{-\pi/h}^{\pi/h} e^{i\xi x_j} \hat{v}(\xi) d\xi. \quad (10)$$

The pair of transforms (9) and (10) are inverse to each other, which is equivalent to the identity (in the sense of distributions)

$$\frac{h}{2\pi} \sum_{j=-\infty}^{\infty} e^{i\xi x_j} = \delta(\xi), \quad \xi \in (-\pi/h, \pi/h), \quad (11)$$

where  $\delta(\xi)$  is the Dirac delta function. This pair can also be viewed as the reverse of Fourier series [51, Chapter 2], though here the grid size  $h$  appears explicitly in both the physical domain  $\mathbb{Z}_h$  and the spectral domain  $I_h$ .

We now state the well-known convolution theorem, whose proof is standard in Fourier Analysis.

*Lemma 2.1* (Convolution as a multiplier in the spectral space). Let  $v, w$  be functions in  $\ell^2(\mathbb{Z}_h)$  and their semi-discrete Fourier transform  $\hat{v}, \hat{w}$  be functions in  $L^2(I_h)$ . Define the operator  $\mathcal{D} : \ell^2(\mathbb{Z}_h) \rightarrow \ell^\infty(\mathbb{Z}_h)$  by

$$(\mathcal{D}v)_j = h \sum_{k=-\infty}^{\infty} v_{j-k} w_k,$$

then the representation of  $\mathcal{D}$  in spectral space is a multiplication of  $\hat{v}$  by  $\hat{w}$ , that is,

$$\widehat{\mathcal{D}v}(\xi) = \hat{w}(\xi)\hat{v}(\xi).$$

Before establishing the connection between the weights and the symbol, we make the following observation. Since the precise value of  $w_0$  in (FLh) is irrelevant (its coefficient is identically zero), without loss of generality in this paper we set

$$w_0 = - \sum_{k \neq 0} w_k. \quad (12)$$

Using this convention, the operator (FLh) becomes a discrete convolution

$$(-\Delta_h)^{\alpha/2} u_j = - \sum_{j=-\infty}^{\infty} u_{j-k} w_k. \quad (\text{FLh}')$$

## 2.2 Spectral representation of the schemes (FLh)

Next we obtain the representation of the general scheme (FLh) in the spectral space, as a direct application of Lemma 2.1.

*Lemma 2.2.* Let  $u$  and  $w$  be functions in  $\ell^2(\mathbb{Z}_h)$ , then the general scheme (FLh) is a multiplication in spectral space, that is

$$\widehat{(-\Delta_h)^{\alpha/2} u}(\xi) = M_h(\xi)\hat{u}(\xi), \quad (13)$$

with the symbol  $M_h(\xi) = -\hat{w}(\xi)/h$ .

The structure of the symbol  $M_h(\xi)$  can be further simplified by isolating the grid size  $h$ . Since  $(-\Delta)^{\alpha/2}$  is a spatial derivative of order  $\alpha$ , it is reasonable to assume that the only dependence of the weights  $\{w_k\}_{k=-\infty}^{\infty}$  on  $h$  is the factor  $h^{-\alpha}$ . Stated differently,  $h^\alpha w_k$  does not depend on  $h$ . As a result, it is more convenient to consider the following rescaled,  $h$ -independent symbol

$$M(\xi) = h^\alpha M_h(\xi/h) = -h^\alpha \sum_{k=-\infty}^{\infty} w_k e^{-ik\xi}, \quad (14)$$

which is defined on the fixed interval  $[-\pi, \pi]$ . We will focus on the rescaled symbol  $M(\xi)$  instead of  $M_h(\xi)$  in the rest of the paper.

On the other hand, if  $M(\xi)$  (or equivalently  $M_h$ ) is known, the corresponding weights  $\{w_k\}_{k=-\infty}^{\infty}$  can be obtained using the inverse transform (10), that is,

$$w_k = -\frac{h}{2\pi} \int_{-\pi/h}^{\pi/h} M_h(\xi) e^{i\xi x_k} d\xi = -\frac{h^{-\alpha}}{\pi} \int_0^\pi M(\xi) \cos(k\xi) d\xi, \quad k \neq 0, \quad (15)$$

where the symmetry  $M(-\xi) = M(\xi)$ , as a result of the fact  $w_k = w_{-k}$ , is used. Therefore, one can develop finite difference schemes of the form (FLh) by proposing appropriate symbols  $M(\xi)$ , provided that the oscillatory integral (15) defining the weights can be evaluated accurately, by either reducing to closed form expression or using numerical quadrature.

*Remark.* If  $M(\xi)$  is continuous at the origin and  $M(0) = 0$ , then  $w_0$  calculated from (15) with  $k = 0$  satisfies the convention  $w_0 = -\sum_{k \neq 0} w_k$  automatically. This fact can be verified easily using the identity (11), since

$$\sum_{k=-\infty}^{\infty} w_k = -\frac{h}{2\pi} \int_{-\pi/h}^{\pi/h} M_h(\xi) \left( \sum_{k=-\infty}^{\infty} e^{i\xi x_k} \right) d\xi = -\int_{-\pi/h}^{\pi/h} M_h(\xi) \delta(\xi) d\xi = 0.$$

Once the one-to-one correspondence between the weights and the symbol as illustrated in (14) and (15) is clear, we can examine the (rescaled) symbols of existing schemes on one hand and propose new schemes from the symbols on the other hand. Before going into these details, we show that many discrete identities and inequalities can be established as a direct consequence of the special form the scheme (FLh), which is often independent of the particular choices of the weights (or the symbols).

### 3 Discrete identities and inequalities

Because of the similar structure between the singular integral (2) and the discrete scheme (FLh), many important identities and inequalities of the continuous operator have their discrete counterparts. These identities are valid under mild conditions on the decay of the discrete functions involved, while the inequalities usually require non-negativity of the weights  $w_k$  with  $k \neq 0$ .

By the definitions of the inner product (7) and the pair of transforms (9) and (10), the following Parseval's identity holds.

*Lemma 3.1* (Parseval's identity). Let  $u$  and  $v$  be two functions in  $\ell^2(\mathbb{Z}_h)$  and  $\hat{u}, \hat{v} \in L^2(I_h)$  be their semi-discrete Fourier transforms. Then

$$\langle u, v \rangle_{\ell^2(\mathbb{Z}_h)} = \frac{1}{2\pi} \langle \hat{u}, \hat{v} \rangle_{L^2(I_h)},$$

and in particular  $\|u\|_{\ell^2(\mathbb{Z}_h)} = \frac{1}{\sqrt{2\pi}} \|\hat{u}\|_{L^2(I_h)}$ .

Similar to the continuous fractional Laplacian, the discrete operator  $(-\Delta_h)^{\alpha/2}$  is also self-adjoint.

*Lemma 3.2.* Let  $u$  and  $v$  be two functions in  $\ell^2(\mathbb{Z}_h)$  such that  $u_j$  and  $v_j$  decay to zero fast enough as  $|j| \rightarrow \infty$ , then

$$\langle (-\Delta_h)^{\alpha/2} u, v \rangle_{\ell^2(\mathbb{Z}_h)} = \langle u, (-\Delta_h)^{\alpha/2} v \rangle_{\ell^2(\mathbb{Z}_h)}.$$

This lemma can be proved easily using the equivalent definition (FLh') and the fact that the weights  $w_k$  are real and symmetric. The inner product in this lemma also suggests the discrete energy  $\mathcal{E}[u] = \frac{1}{2} \langle (-\Delta_h)^{\alpha/2} u, u \rangle_{\ell^2(\mathbb{Z}_h)}$ , that is,

$$\mathcal{E}[u] = \frac{h}{4} \sum_{j=-\infty}^{\infty} \sum_{k=-\infty}^{\infty} |u_j - u_{j-k}|^2 w_k, \quad (16)$$

or equivalently

$$\mathcal{E}[u] = \frac{1}{4\pi} \int_{-\pi/h}^{\pi/h} M_h(\xi) |\hat{u}(\xi)|^2 d\xi. \quad (17)$$

Therefore, from the expressions (16) and (17), the energy is non-negative under certain conditions, as summarized in the following lemma.

*Lemma 3.3.* If either the symbol  $M(\xi)$  or the weights  $w_k$  ( $k \neq 0$ ) are non-negative, then the energy  $\mathcal{E}[u]$  is non-negative.

The following inequalities are useful in various estimates for the analysis of differential equation where the fractional Laplacian is discretised with the scheme (FLh), motivated from their continuous counterparts initiated in the study of the quasi-geostrophic equation by Córdoba and Córdoba [13, 14] and then generalized by Ju [31].

*Lemma 3.4.* Let  $\alpha \in (0, 2)$ ,  $p > 1$  and  $u, v$  be functions defined on the grid  $\mathbb{Z}_h$  such that  $v_j = |u_j|^p$ . If the weights  $\{w_k\}_{k=-\infty}^{\infty}$  are non-negative for  $k \neq 0$ , the following point estimate holds

$$|u_j|^{p-2} u_j (-\Delta_h)^{\alpha/2} u_j \geq \frac{1}{p} (-\Delta_h)^{\alpha/2} v_j.$$

*Proof.* From Young's inequality, for any  $u_j$  and  $u_{j-k}$ ,

$$\frac{p-1}{p} |u_j|^p + \frac{1}{p} |u_{j-k}|^p \geq |u_j|^{p-1} |u_{j-k}| \geq |u_j|^{p-2} u_j u_{j-k},$$

which is equivalent to

$$|u_j|^{p-2} u_j (u_j - u_{j-k}) \geq \frac{1}{p} (|u_j|^p - |u_{j-k}|^p) = \frac{1}{p} (v_j - v_{j-k}).$$

Therefore, from the definition of the discrete operator,

$$\begin{aligned} |u_j|^{p-2} u_j (-\Delta_h)^{\alpha/2} u_j &= \sum_{k \neq 0} |u_j|^{p-2} u_j (u_j - u_{j-k}) w_k \\ &\geq \frac{1}{p} \sum_{k \neq 0} (|u_j|^p - |u_{j-k}|^p) w_k = \frac{1}{p} (-\Delta_h)^{\alpha/2} v_j. \end{aligned}$$

□

This lemma can be used to prove the discrete version of the Stroock-Varopoulos inequality.



*Lemma 3.5.* Let  $\alpha \in (0, 2)$  and  $p > 2$ . If both the function  $u$  and its discrete fractional Laplacian  $(-\Delta_h)^{\alpha/2}u$  are defined on  $\mathbb{Z}_h$ ,

$$\langle |u|^{p-2}u, (-\Delta_h)^{\alpha/2}u \rangle_{\ell^2(\mathbb{Z}_h)} \geq \frac{2}{p} \langle |u|^{p/2}, (-\Delta_h)^{\alpha/2}|u|^{p/2} \rangle_{\ell^2(\mathbb{Z}_h)}.$$

*Proof.* Similarly by Young's inequality,

$$\frac{p-2}{p}|u_j|^{\frac{p}{2}} + \frac{2}{p}|u_{j-k}|^{\frac{p}{2}} \geq |u_j|^{\frac{p}{2}-1}|u_{j-k}| \geq |u_j|^{\frac{p}{2}-2}u_ju_{j-k},$$

which can be rearranged as

$$|u_j|^p - |u_j|^{p-2}u_ju_{j-k} \geq \frac{2}{p}|u_j|^{\frac{p}{2}}(|u_j|^{\frac{p}{2}} - |u_{j-k}|^{\frac{p}{2}}).$$

Therefore,

$$\begin{aligned} \langle |u|^{p-2}u, (-\Delta_h)^{\alpha/2}u \rangle_{\ell^2(\mathbb{Z}_h)} &= h \sum_j \sum_{k \neq 0} |u_j|^{p-2}u_j(u_j - u_{j-k})w_k \\ &\geq \frac{2h}{p} \sum_j \sum_{k \neq 0} |u_j|^{\frac{p}{2}}(|u_j|^{\frac{p}{2}} - |u_{j-k}|^{\frac{p}{2}})w_k = \frac{2}{p} \langle |u|^{p/2}, (-\Delta_h)^{\alpha/2}|u|^{p/2} \rangle_{\ell^2(\mathbb{Z}_h)}. \end{aligned}$$

□

When the scheme (FLh) is used to discretise the fractional Laplacian operator in differential equations, above identities or inequalities are critical to establish similar energy estimates and other qualitative properties as in the continuous settings. If the original differential equation is derived from variational principles, the discretised equation can also be obtained from discrete variational principles involving the energy  $\mathcal{E}$ . Consequently, the analogy between the continuous operator and its discretization (FLh) allows the development of a parallel theory or method in both settings. However, we will focus on practical numerical aspects below and leave further investigations related to these discrete estimates as future work.

## 4 Presentation of the weights

In this section we present several finite difference approximations of the fractional Laplacian operator of the form (FLh), including schemes constructed from explicit symbols like  $|\xi|^\alpha$  or  $(2 - 2 \cos \xi)^{\alpha/2}$ , a variant of the Grünwald-Letnikov method associated with fractional derivatives, and quadrature-difference methods based on the singular integral (2). The focus of this section is on the derivation of the weights or the associated symbols, while other important properties are summarised and compared in the next section.

*Remark.* The expressions of the weights  $w_k$  for different schemes are usually only given for  $k > 0$ , with the assumption that  $w_k = w_{-k}$  for  $k < 0$  and  $w_0 = -\sum_{k \neq 0} w_k$ , although some formulas are still valid for negative indices  $k$ . When the weights or the symbols are referred for a particular method, superscripts are used to label and distinguish them. For instance,  $w_k^{SP}$  and  $M^{SP}(\xi)$  are the weights and the associated rescaled symbol for the spectrally accurate scheme discussed in the next subsection.

## 4.1 Spectral weights and sinc interpolation

Spectral methods are widely used in scientific computing [7, 46, 51], where the functions involved are expanded using basis defined on the whole computational domain. Classical derivatives are usually evaluated with Fast Fourier Transform (FFT), and the error decays exponentially fast for smooth functions, hence so call the *spectral accuracy*. For functions define on the whole space with fast decay at infinity, similar error properties are preserved when the computational domain is truncated to be finite.

The fractional Laplacian operator, as a multiplier in the spectral space, can be evaluated using FFT-based spectral methods, which is still spectrally accurate for smooth *periodic* functions. However, if the function  $u$  is defined on the whole real line, the nonlocality of the operator has a non-trivial effect: when the computational domain is truncated to be  $[-L, L]$  for some finite  $L > 0$ , the error of the conventional Fourier spectral method decays only algebraically (on the domain size  $L$ ), even  $u$  approaches zero fast at infinity. In fact, the result returned from FFT is  $(-\Delta)^{\alpha/2}\tilde{u}(x)$  instead of  $(-\Delta)^{\alpha/2}u(x)$ , where  $\tilde{u}$  is the period extension of  $u$  from the interval  $[-L, L]$  to the whole real line, i.e.,

$$\tilde{u}(x) = \sum_{j=-\infty}^{\infty} u(x - 2jL).$$

More precisely, if  $u$  is essentially supported on the interval  $[-L, L]$ , the leading order error is

$$(-\Delta)^{\alpha/2}\tilde{u}(x) - (-\Delta)^{\alpha/2}u(x) = -C_{1,\alpha} \sum_{j \neq 0} \int_{\mathbb{R}} \frac{u(x - 2jL)}{|x - y|^{1+\alpha}} dy = O(L^{-1-\alpha}),$$

for  $x \in (-L, L)$ . This algebraically slow convergence is shown in Figure 4.1(a) for  $u(x) = e^{-x^2}$ , whose fractional Laplacian at the origin can be calculated explicitly as

$$(-\Delta)^{\alpha/2}u(0) = \frac{1}{\sqrt{\pi}} \int_0^{\infty} k^{\alpha} e^{-k^2/4} dk = 2^{\alpha} \Gamma\left(\frac{1+\alpha}{2}\right) / \sqrt{\pi}.$$

The leading  $O(L^{-1-\alpha})$  error at the origin is also verified numerically in Figure 4.1(b).

While the conventional Fourier spectral method is not satisfactory as expected, the correct one in the form of (FLh) can be constructed by choosing the exact symbol  $M(\xi) = |\xi|^{\alpha}$ . In this way, the weights defined via (15) become

$$w_k^{SP} = -\frac{h^{-\alpha}}{\pi} \int_0^{\pi} \xi^{\alpha} \cos(k\xi) d\xi. \quad (18)$$

Exactly the same weights  $w_k^{SP}$  can be derived alternatively from the well-known sinc interpolation  $\mathcal{P}u$  of  $u$ , when  $(-\Delta)^{\alpha/2}u(x_j)$  is approximated by  $(-\Delta)^{\alpha/2}\mathcal{P}u(x_j)$ . Here the sinc interpolation  $\mathcal{P}u$  is defined by

$$\mathcal{P}u(x) = \sum_{k=-\infty}^{\infty} u_k \operatorname{sinc} \frac{x - x_k}{h},$$

with the sinc function  $\operatorname{sinc} x = \frac{\sin \pi x}{\pi x}$  that has been explored extensively for the numerical solutions of differential equations [37, 49]. The function  $\mathcal{P}u$  is an interpolation of  $u$  on  $\mathbb{R}$  in

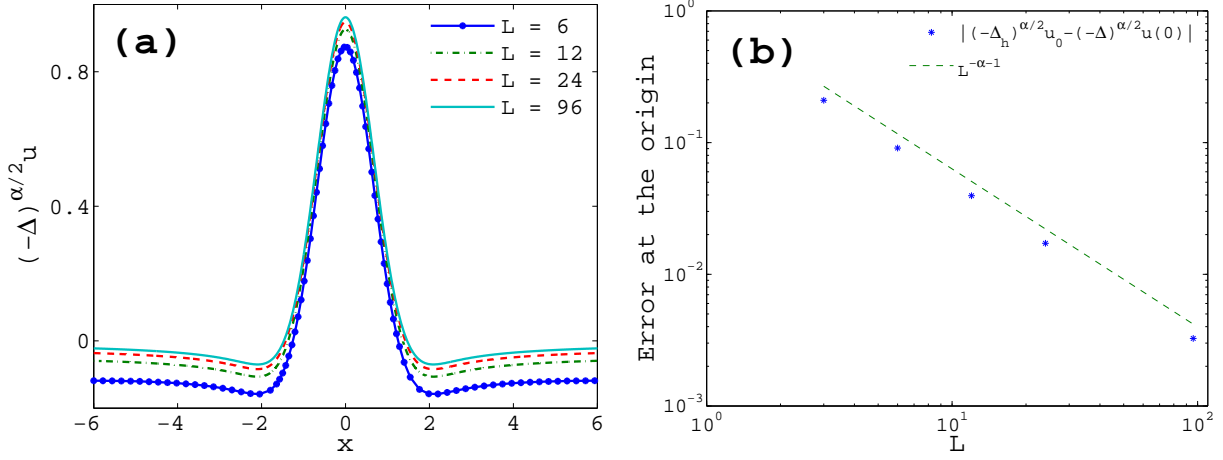


Figure 4.1: The slow convergence of the fractional Laplacian based on FFT: (a) the fractional Laplacian of  $u(x) = e^{-x^2}$  for  $\alpha = 0.2$  computed on different domain sizes (but only shown on  $[-6, 6]$ ); (b) the error at the origin that decays like  $O(L^{-\alpha-1})$ .

the sense that  $\mathcal{P}u(x_j) = u_j$  for any  $j \in \mathbb{Z}$ . Once  $\mathcal{P}u$  is defined, the same weights (18) can be derived, using the crucial property that the Fourier transform of  $\text{sinc } x$  is precisely  $\chi_{[-\pi, \pi]}(\xi)$ , the characteristic function on  $[-\pi, \pi]$ . In this way, the Fourier transform of  $\mathcal{P}u$  is

$$\mathcal{F}[\mathcal{P}u](\xi) = h\chi_{[-\pi/h, \pi/h]}(\xi) \sum_{k=-\infty}^{\infty} u_k e^{-i\xi x_k}$$

and the discrete operator defined by  $(-\Delta)^{\alpha/2}[\mathcal{P}u](x_j)$  can be written as

$$\frac{1}{2\pi} \int_{-\infty}^{\infty} e^{i\xi x_j} |\xi|^\alpha \mathcal{F}[\mathcal{P}u](\xi) d\xi = \frac{h}{2\pi} \int_{-\pi/h}^{\pi/h} \left( \sum_{k=-\infty}^{\infty} u_k e^{i\xi(x_j - x_k)} \right) |\xi|^\alpha d\xi.$$

Finally using the identity (11), we get

$$\frac{h}{2\pi} \int_{-\pi/h}^{\pi/h} \left( \sum_{k=-\infty}^{\infty} u_j e^{i\xi(x_j - x_k)} \right) |\xi|^\alpha d\xi = u_j e^{i\xi x_j} \int_{-\pi/h}^{\pi/h} \left( \frac{h}{2\pi} \sum_{k=-\infty}^{\infty} e^{-i\xi x_k} \right) |\xi|^\alpha d\xi = 0.$$

Therefore, by combining the previous two equations,  $(-\Delta)^{\alpha/2}[\mathcal{P}u](x_j)$  can be simplified as

$$\begin{aligned} & \frac{h}{2\pi} \int_{-\pi/h}^{\pi/h} \left( \sum_{k=-\infty}^{\infty} u_k e^{i\xi(x_j - x_k)} \right) |\xi|^\alpha d\xi - \frac{h}{2\pi} \int_{-\pi/h}^{\pi/h} \left( \sum_{k=-\infty}^{\infty} u_j e^{i\xi(x_j - x_k)} \right) |\xi|^\alpha d\xi \\ &= \sum_{k=-\infty}^{\infty} (u_k - u_j) \frac{h}{2\pi} \int_{-\pi/h}^{\pi/h} e^{i\xi(x_k - x_j)} |\xi|^\alpha d\xi \\ &= - \sum_{k=-\infty}^{\infty} (u_j - u_{j-k}) \frac{h^{-\alpha}}{2\pi} \int_{-\pi}^{\pi} |\xi|^\alpha \cos k\xi d\xi. \end{aligned}$$

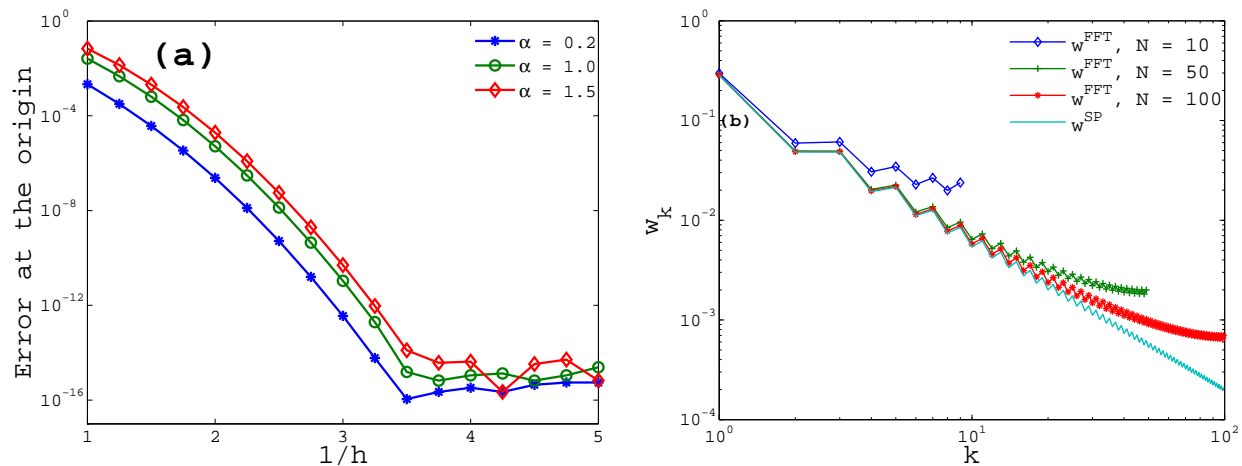


Figure 4.2: (a) The spectral accuracy of the spectral weights  $w^{SP}$  for the fractional Laplacian of  $e^{-x^2}$  at the origin  $\alpha = 0.2$  with  $\alpha = 1.0$  and  $\alpha = 1.5$ . (b) The spectral weights  $w^{SP}$  and the weights extracted from FFT (normalized by the grid size  $h^\alpha$ ) for  $\alpha = 0.5$ .

Comparing the last expression with (FLh), we recover the same weights  $w_k^{SP}$  given by (18). Since the symbol  $M^{SP}(\xi)$  is exactly  $|\xi|^\alpha$ , we call  $w^{SP}$  the spectral weights.

The spectral convergence rate of the weights  $w^{SP}$  is verified in Figure 4.2(a), for the fractional Laplacian of  $u(x) = e^{-x^2}$  at the origin with different  $\alpha$ . The computational domain is fixed to be  $[-8, 8]$  and the accuracy does not improve on larger domains for fixed grid size  $h$ . By a careful analysis, FFT-based scheme for the fractional Laplacian also takes the form (FLh), and the weights<sup>1</sup> are trapezoidal rule approximation of the integral (18). Consequently, the weights from FFT-based scheme converge to the spectral weights when the number of points used in FFT goes to infinity, as shown in 4.2(b).

*Remark.* When  $k$  is large, it is difficult to evaluate highly oscillatory integrals like (18) accurately, and alternative expressions using special functions are preferred. In terms of the lower incomplete Gamma function  $\gamma(a, z) = \int_0^z t^{a-1} e^{-t} dt$ , the anti-derivative of  $\xi^\alpha e^{ik\xi}$  can be evaluated as  $(-ik)^{-\alpha-1} \gamma(\alpha + 1, -ik\xi)$ . Hence the integral (18) can be written as

$$\begin{aligned} w_k^{SP} &= \frac{h^{-\alpha}}{\pi} \operatorname{Re}((-ik)^{-\alpha-1} [\Gamma(\alpha + 1, -\pi ik) - \Gamma(\alpha + 1, 0)]) \\ &= -\frac{h^{-\alpha} \pi^\alpha}{\alpha + 1} \operatorname{Re}({}_1F_1(\alpha + 1; \alpha + 2; ik\pi)), \end{aligned} \quad (19)$$

in terms of confluent hypergeometric function  ${}_1F_1$ . These special functions involved can be evaluated much more efficiently with existing packages [21, 56].

*Remark.* The weights  $w_k^{SP}$  for  $\alpha = 1$  or  $2$  can be obtained in elementary means, that is,

$$w_k^{SP} = \begin{cases} (1 - (-1)^k)/k^2 \pi h, & \alpha = 1, \\ 2(-1)^{k+1}/k^2 h^2, & \alpha = 2, \end{cases} \quad (20)$$

<sup>1</sup>These weights can be taken as the output of the FFT-based method on the discrete Dirac delta function.

where the case  $\alpha = 2$  already appeared in [51, equation (2.14)] for spectrally accurate discretization of the second derivative. These special cases indicate that the desired non-negativity of the weights may be lost; in fact, it can be shown numerically that the weights have alternating signs for  $\alpha$  between 1 and 2.

## 4.2 Weights from regularized Fourier symbol

The above scheme with the spectral weights  $\{w_k^{SP}\}$ , despite its high accuracy for smooth functions, has some undesired properties. Because of the presence of negative weights for  $\alpha > 1$ , the discrete fractional Laplacian of functions defined on  $\mathbb{Z}_h$  is not necessarily negative at its global maximum. Negative densities could arise in the explicit Euler scheme (6) for the fractional heat equation. Moreover, in the limit as  $\alpha$  approaches  $2^-$ , the scheme with limiting weights shown in (20) does not agree with any common finite difference approximation of  $-\partial_{xx}$  on a compact stencil.

On the other hand, to reinforce the limiting behaviour as  $\alpha \rightarrow 2^-$ , the general scheme can be constructed as follow: take the symbol at  $\alpha = 2$  and define the new symbol for  $\alpha \in (0, 2)$  by raising to power  $\alpha/2$ . For instance, the rescaled symbol to the standard three-point central difference method of  $-\partial_{xx}$  is  $2(1 - \cos(\xi))$  and thus the symbol for general  $\alpha$  between 0 and 2 is just

$$M^{PER}(\xi) = [2(1 - \cos(\xi))]^{\alpha/2}, \quad (21)$$

with the weights

$$w_k^{PER} = -\frac{h^{-\alpha}}{\pi} \int_0^\pi [2(1 - \cos(\xi))]^{\alpha/2} \cos(k\xi) d\xi.$$

In fact, these weights have already been calculated explicitly in [57, equation (7)],

$$w_k^{PER} = h^{-\alpha} \frac{\Gamma(k - \frac{\alpha}{2})\Gamma(1 + \alpha)}{\pi\Gamma(k + 1 + \frac{\alpha}{2})} \sin\left(\frac{\alpha\pi}{2}\right), \quad k > 0. \quad (22)$$

Since  $\Gamma(z) > 0$  for any  $z > 0$ , this closed form expression clearly shows the non-negativity of the weights for  $\alpha \in (0, 2)$ .

Following the same spirit, other schemes can be constructed based on higher order difference approximation of  $-\partial_{xx}$ . For example, from the five-point central difference

$$-u''(x_j) \approx \frac{1}{h^2} \left( \frac{1}{12}u(x_j + 2h) - \frac{4}{3}u(x_j + h) + \frac{5}{2}u(x_j) - \frac{4}{3}u(x_j - h) + \frac{1}{12}u(x_j - 2h) \right),$$

we can choose  $M(\xi) = \left(\frac{5}{2} - \frac{8}{3}\cos\xi + \frac{1}{6}\cos 2\xi\right)^{\alpha/2}$ . However, this approach of pursuing higher order schemes is limited for at least two reasons. First, the resulting weights may become negative when  $\alpha$  is close to 2. Second, the integral (15) defining the weights from the symbol is highly oscillatory for large  $k$ , and the error in the evaluation of the weights can contaminate the accuracy of the underlying scheme, unless closed form expressions like (18) or (22) are available.

*Remark.* The superscript *PER* is chosen because the rescale symbol  $M^{PER}(\xi)$  can be extended smoothly as a periodic function near the boundary  $\pm\pi$  (though still not smooth near the origin).

### 4.3 Gorenflo-Mainardi scheme using Grünwald-Letnikov weights

In one dimension, the fractional Laplacian can be expressed as the symmetric combination of two fractional derivatives as in (4), and hence numerical schemes for fractional Laplacians can be constructed from the classical Grünwald-Letnikov differences originated from fractional derivatives. The corresponding weights, proposed by Gorenflo and Mainardi [23, 22, 24], are given by

$$w_k^{GL} = \frac{h^{-\alpha}}{2 \cos(\alpha\pi/2)} \frac{\alpha \Gamma(k - \alpha)}{k! \Gamma(1 - \alpha)}, \quad k \geq 1, \quad (23a)$$

for  $\alpha \in (0, 1)$  and

$$w_k^{GL} = \begin{cases} -\frac{h^{-\alpha}}{2 \cos(\alpha\pi/2)} \left[1 + \alpha(\alpha - 1)/2\right], & k = 1, \\ \frac{h^{-\alpha}}{2 \cos(\alpha\pi/2)} \frac{\alpha \Gamma(k+1-\alpha)}{(k+1)! \Gamma(1-\alpha)}, & k > 1, \end{cases} \quad (23b)$$

for  $\alpha \in (1, 2]$ . Notice that the weights in the range  $\alpha \in (1, 2)$  are just a simple shift of those for  $\alpha \in (0, 1)$ , to preserve the non-negativity of the weights and therefore many other desired properties. The case  $\alpha = 1$  is handled separately, because it can not be continued from the above two cases (23a) and (23b) by taking the limits  $\alpha \rightarrow 1^-$  and  $\alpha \rightarrow 1^+$  respectively; for this special case, one option is to choose (see [24] for more details)

$$w_k^{GL} = \frac{1}{\pi h} \frac{1}{k(k+1)}, \quad k > 0.$$

The rescaled symbol  $M^{GL}(\xi)$  associated with the weights (23a) and (23b) can be computed explicitly, based on the binomial expansion of  $(1 - z)^\alpha$ . That is,

$$(1 - z)^\alpha = 1 - \frac{\alpha}{\Gamma(1 - \alpha)} \sum_{k=1}^{\infty} \frac{\Gamma(k - \alpha)}{k!} z^k \quad (24a)$$

$$= 1 - \alpha z + \frac{1}{2} \alpha(\alpha - 1) z^2 - \frac{\alpha}{\Gamma(1 - \alpha)} \sum_{k=2}^{\infty} \frac{\Gamma(k + 1 - \alpha)}{(k + 1)!} z^{k+1}. \quad (24b)$$

By substituting  $z = 1$  into (24a) and (24b), we obtain

$$w_0^{GL} = - \sum_{k \neq 0} w_k^{GL} = \begin{cases} -[h^\alpha \cos(\alpha\pi/2)]^{-1}, & \alpha \in (0, 1), \\ \alpha[h^\alpha \cos(\alpha\pi/2)]^{-1}, & \alpha \in (1, 2]. \end{cases} \quad (25)$$

Once  $w_0^{GL}$  is determined, the rescaled symbol  $M(\xi)$  is obtained by rearranging the terms in (24a) and (24b) with  $z = e^{\pm i\xi}$ , that is,

$$M^{GL}(\xi) = -h^\alpha \sum_{k=-\infty}^{\infty} e^{-ik\xi} w_k^{GL} = \begin{cases} \frac{1}{2 \cos \alpha\pi/2} [(1 - e^{i\xi})^\alpha + (1 - e^{-i\xi})^\alpha], & \alpha \in (0, 1), \\ \frac{1}{2 \cos \alpha\pi/2} [e^{-i\xi}(1 - e^{i\xi})^\alpha + e^{i\xi}(1 - e^{-i\xi})^\alpha], & \alpha \in (1, 2]. \end{cases}$$

Here the branch of the multivalued functions  $(1 - e^{\pm i\xi})^\alpha$  are chosen so that it is consistent with the expansions (24a) and (24b). Using trigonometric identities,  $M^{GL}(\xi)$  can be further simplified as

$$M^{GL}(\xi) = \begin{cases} \frac{\cos \frac{\pi - |\xi|}{2} \alpha}{\cos \frac{\alpha\pi}{2}} \left(2 \sin \frac{|\xi|}{2}\right)^\alpha, & \alpha \in (0, 1), \\ \frac{\cos(\frac{\pi - |\xi|}{2} \alpha + |\xi|)}{\cos \frac{\alpha\pi}{2}} \left(2 \sin \frac{|\xi|}{2}\right)^\alpha, & \alpha \in (1, 2]. \end{cases} \quad (26)$$

However, this approach based on fractional derivatives is restricted to be in one dimension. The straightforward extension to  $\mathbb{R}^n$  by taking summations of fractional Laplacian in each dimension gives rise to the symbol  $|\xi_1|^\alpha + |\xi_2|^\alpha + \cdots + |\xi_n|^\alpha$ , different from the one  $|\xi|^\alpha = (|\xi_1|^2 + \cdots + |\xi_n|^2)^{\alpha/2}$  of our interests here.

#### 4.4 The finite difference-quadrature method

Finally we discuss the weights derived from quadratures based on the singular integral representation (2). This approach has been taken in the context of finite volume or finite difference methods [18, 11, 12], where  $u$  is assumed to be the constant  $u(x_j)$  on the interval  $(x_j - h/2, x_j + h/2)$ . In this way,

$$\begin{aligned} (-\Delta)^{\alpha/2} u(x_j) &= C_{1,\alpha} \sum_{k=-\infty}^{\infty} \int_{x_{j-k}-h/2}^{x_{j-k}+h/2} |x_j - y|^{-1-\alpha} (u(x_j) - u(y)) \, dy \\ &\approx \sum_{k \neq 0} (u_j - u_{j-k}) C_{1,\alpha} \int_{x_{j-k}-h/2}^{x_{j-k}+h/2} |x_j - y|^{-1-\alpha} \, dy, \end{aligned}$$

from which the weights  $w_k$  can be extracted. However, the singularity when  $y \approx x_j$  is in general not treated appropriately, leading to inconsistency as  $\alpha$  goes to  $2^-$  (a recent correction is made in [19]).

An improved difference-quadrature scheme is proposed by the authors in [27], using piecewise local polynomial basis. Near the singularity  $y \approx x_j$  in the integral (2),  $u(y)$  is replaced by the (second order) Taylor expansion of  $u(x)$  at  $x_j$ , while away from the singularity,  $u(y)$  is approximated by piecewise linear or quadratic polynomials. Here we only quote the expressions of the weights and refer to [27] for more details. Define the auxiliary functions  $F(t)$  and  $G(t)$  such that  $F''(t) = G'''(t) = t^{-1-\alpha}$ , or equivalently,

$$F(t) = \begin{cases} \frac{1}{(\alpha-1)\alpha} |t|^{1-\alpha}, & \alpha \neq 1 \\ -\log |t|, & \alpha = 1 \end{cases}, \quad G(t) = \begin{cases} \frac{1}{(2-\alpha)(\alpha-1)\alpha} |t|^{2-\alpha}, & \alpha \neq 1 \\ t - t \log |t|, & \alpha = 1 \end{cases}.$$

Then the weights using piecewise linear functions (Tent functions) are given by

$$w_k^T = C_{1,\alpha} h^{-\alpha} \begin{cases} \frac{1}{2-\alpha} - F'(1) + F(2) - F(1), & k = 1, \\ F(k+1) - 2F(k) + F(k-1), & k = 2, 3, \dots, \end{cases}$$

and the weights using piecewise quadratic functions are given by

$$\frac{h^\alpha w_k^Q}{C_{1,\alpha}} = \begin{cases} \frac{1}{2-\alpha} - G''(1) - \frac{G'(3) + 3G'(1)}{2} + G(3) - G(1), & k = 1, \\ 2[G'(k+1) + G'(k-1) - G(k+1) + G(k-1)], & k = 2, 4, 6, \dots, \\ -\frac{G'(k+2) + 6G'(k) + G'(k-2)}{2} + G(k+2) - G(k-2), & k = 3, 5, 7, \dots. \end{cases}$$

Piecewise cubic or higher order polynomials can also be used, but the resulting weights may also become negative (not surprisingly again when  $\alpha$  is close to 2) and hence further study

in this direction is not pursued. Different from the previous three cases, the rescaled symbol  $M(\xi)$  for either  $w_k^T$  or  $w_k^Q$  does not seem to possess a closed form expression.

With different weights and their symbols in mind, we are now in a position to compare them so that we can chose the right one in practice.

## 5 Discussions and Comparisons of the weights

In this section we compare and discuss more specific properties of the weights presented in the last section, especially their order of accuracy, ultimately important for different choices of the schemes.

### 5.1 Basic properties of the weights

Properties shared by most of the schemes are discussed in this subsection, including positivity, asymptotic decay rates as the indices go to infinity, the limiting behaviours as  $\alpha$  goes to 2 and CFL conditions in the discretisation of evolution equations. The orders of accuracy of these schemes are discussed in the next subsection, using a local expansion of the rescaled symbol  $M(\xi)$ .

#### Positivity and decay rate

The non-negativity of the weights (except  $w_0$ ) is essential in practical discretisation of elliptic or parabolic PDEs to preserve the discrete maximum principle or comparison principle. The weights  $w^{PER}$  and  $w^{GL}$  are clearly positivity, from the explicit formulas of the weights (22), (23a) and (23b). The weights  $w^T$  and  $w^Q$  are also shown to be strictly positive in [27], but not necessarily true when higher order polynomial interpolations are used. In contrast, the weights  $w^{SP}$  are strictly positive only for  $\alpha \in (0, 1)$ ; when  $\alpha \in (1, 2)$ ,  $w_k^{SP}$  is negative for  $k$  even, making it less attractive in many applications despite its spectral accuracy.

The asymptotic decay rates of these weights  $w_k$  as the index  $k$  goes to infinity can also be obtained. From asymptotic expansion  $\Gamma(z) \sim \sqrt{2\pi}z^{z-1/2}e^{-z}$  for Gamma function  $\Gamma(z)$  with large argument  $z$  [1], it is easy to see that  $\Gamma(z+a)/\Gamma(z+b) \sim z^{a-b}$  and all three ratios

$$\frac{\Gamma(k - \frac{\alpha}{2})}{\Gamma(k + 1 + \frac{\alpha}{2})}, \quad \frac{\Gamma(k - \alpha)}{k!}, \quad \frac{\Gamma(k + 1 - \alpha)}{(k + 1)!}$$

have the same leading asymptotics  $k^{-\alpha-1}$ . Consequently,

$$w_k^{PER} \sim \frac{\Gamma(1 + \alpha)}{\pi} \sin\left(\frac{\alpha\pi}{2}\right) k^{-\alpha-1} h^{-\alpha} \quad \text{and} \quad w_k^{GL} \sim \frac{\alpha}{2 \cos \frac{\alpha\pi}{2}} \frac{1}{\Gamma(1 - \alpha)} k^{-\alpha-1} h^{-\alpha}.$$

Similarly, from the expressions for  $w^T$  and  $w^Q$  given in the previous section,

$$w_k^T \sim C_{1,\alpha} k^{-\alpha-1} h^{-\alpha}, \quad w_k^Q \sim \begin{cases} \frac{4}{3} C_{1,\alpha} k^{-\alpha-1} h^{-\alpha}, & k \text{ odd,} \\ \frac{2}{3} C_{1,\alpha} k^{-\alpha-1} h^{-\alpha} & k \text{ even.} \end{cases}$$



In fact, the constant prefactors to  $k^{-\alpha-1}h^{-\alpha}$  are exactly the same for all the weights  $w^{PER}$ ,  $w^{GL}$  and  $w^T$ . Using the well-known Euler's reflection formula  $\Gamma(z)\Gamma(1-z) = \pi/\sin z$  and the duplication formula  $\Gamma(z)\Gamma(z + \frac{1}{2}) = 2^{1-2z}\sqrt{\pi}\Gamma(2z)$  [1], we have

$$\frac{\Gamma(1+\alpha)}{\pi} \sin\left(\frac{\alpha\pi}{2}\right) = \frac{\alpha}{2 \cos \frac{\alpha\pi}{2}} \frac{1}{\Gamma(1-\alpha)} = \frac{\alpha 2^{\alpha-1} \Gamma(\frac{1+\alpha}{2})}{\pi^{1/2} \Gamma(\frac{2-\alpha}{2})} (= C_{1,\alpha}).$$

The asymptotic decay rates are more complicated for  $w^{SP}$ . We can show numerically that, for  $\alpha \in (0, 1)$ , the weights  $w_k^{SP}$  have the same scaling  $k^{-\alpha-1}h^{-\alpha}$  as others, while for  $\alpha \in (1, 2)$ , the weights  $w_k^{SP}$  scale like  $k^{-2}h^{-\alpha}$  with alternating signs. The scaling behaviour of the weights is verified in Figure 5.1.

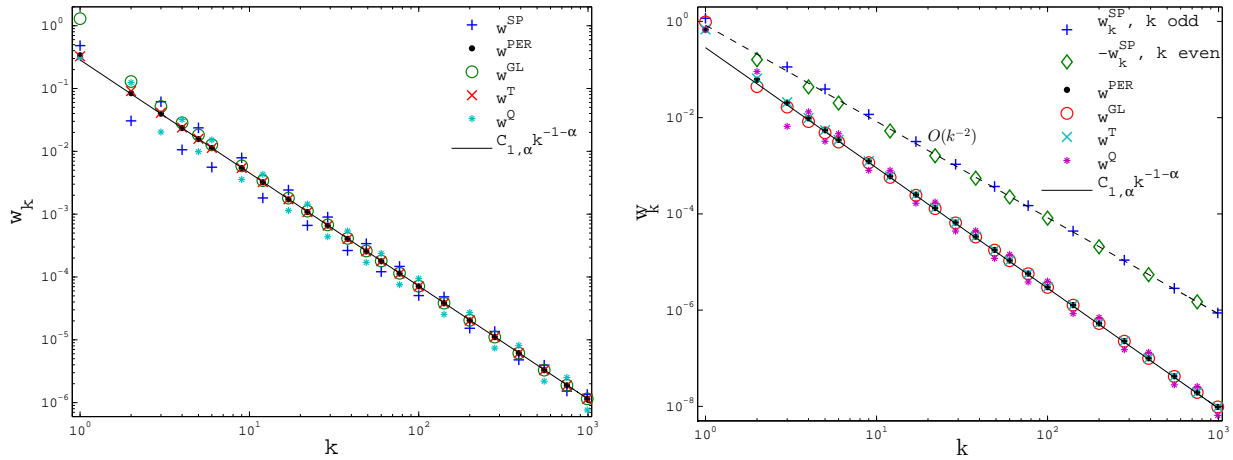


Figure 5.1: The decay of the weights  $w_k$  of different methods (without the factor  $h^{-\alpha}$ ), for (a)  $\alpha = 0.8$  and (b)  $\alpha = 1.5$ . All positive weights decay with the same rate  $k^{-1-\alpha}$ , while the rate for  $w^{SP}$  as  $\alpha \in (1, 2)$  is  $O(k^{-2})$ .

*Remark.* The scaling behaviour of the Fourier integral  $\int_{-\pi}^{\pi} M(\xi)e^{ik\xi} d\xi$  in  $k$  is intimately related to the singularity of  $M(\xi)$  on the interval  $[-\pi, \pi]$ , analogous to the relation between the smoothness of a function and the decay of its Fourier transform (or Fourier series). Using asymptotic analysis on (18), one can show that  $w_k^{SP}$  decays like  $k^{-2}$  for  $\alpha \in (1, 2)$ , instead of the expected rate  $k^{-\alpha-1}$  shared by other weights.

### The limit when $\alpha \rightarrow 2^-$

As  $\alpha$  goes to  $2^-$ , the fractional Laplacian  $(-\Delta)^{\alpha/2}$  becomes the standard (negative) Laplacian. Hence the corresponding numerical scheme (FLh) is expected to converge to some approximation of  $-\partial_{xx}$ , preferably the three-point central difference  $(2u_j - u_{j+1} - u_{j-1})/h^2$ . The limiting weights can be calculated directly from their explicit expressions presented in the last section. From (20),  $w^{SP}$  becomes the spectral method on the whole real line [51]. All other weights  $w^{PER}$ ,  $w^{GL}$ ,  $w^T$  and  $w^Q$  converge to the limiting scheme with  $w_{\pm} = 1$  and  $w_k = 0$  for  $k > 1$ , mainly using the fact that  $\Gamma(z) \approx 1/z$  as  $z \rightarrow 0$ . Therefore, the standard three-point central difference in the limit  $\alpha \rightarrow 2^-$  is recovered for all weights except  $w^{SP}$ .

## CFL condition

When an evolution equation is discretised, the time step is usually restricted by the so called *CFL condition* for stability reason. Taking the fractional heat equation  $u_t + (-\Delta)^{\alpha/2}u = 0$  for example, the forward Euler scheme at time level  $n + 1$  is

$$u_j^{n+1} = (1 + w_0\Delta t)u_j^n + \Delta t \sum_{k \neq 0} w_k u_{j-k}^n.$$

Beside that the weights should be non-negative, the time step is also restricted by the CFL condition  $1 + w_0\Delta t \geq 0$ , i.e.,

$$\frac{\Delta t}{h^\alpha} \leq C_{\max} := -\frac{1}{h^\alpha w_0} = \frac{1}{h^\alpha \sum_{k \neq 0} w_k}.$$

As a result, we examine the special weight  $w_0$  for different schemes below.

If the rescaled symbol  $M(\xi)$  satisfies the condition  $M(0) = 0$ ,  $w_0$  is given directly from the integral (15) (by taking  $k = 0$ ). This immediately implies that

$$w_0^{SP} = -\frac{h^{-\alpha}}{\pi} \int_0^\pi \xi^\alpha d\xi = -\frac{\pi^\alpha}{1 + \alpha} h^{-\alpha},$$

and

$$w_0^{PER} = -\frac{h^{-\alpha}}{\pi} \int_0^\pi [2(1 - \cos \xi)]^{\alpha/2} d\xi = -\frac{4\Gamma(\alpha)}{\alpha\Gamma(\alpha/2)^2} h^{-\alpha},$$

together with  $w_0^{GL}$  already derived in (25). Though the rescaled symbol  $M(\xi)$  is not explicit, the weights  $w^T$  or  $w^Q$  constitute a telescoping series, and

$$w_0^T = w_0^Q = -2C_{1,\alpha} h^{-\alpha} \left[ \frac{1}{2 - \alpha} - F'(1) \right] = -\frac{2^\alpha \Gamma(\frac{1+\alpha}{2})}{\pi^{1/2} \Gamma(2 - \frac{\alpha}{2})} h^{-\alpha}.$$

The constant  $C_{\max} = (-h^\alpha w_0)^{-1} = (h^\alpha \sum_{k \neq 0} w_k)^{-1}$ , as a function of  $\alpha$  is shown in Figure 5.2 for different schemes. It is obvious that the CFL condition becomes too restrictive only for  $w^{GL}$  near  $\alpha = 1$ , where the time step has to be vanishingly small. Because of the alternating signs of the weights  $w_k^{SP}$  for  $\alpha \in (1, 2)$ , the CFL condition is only shown on the interval  $\alpha \in (0, 1)$ .

## 5.2 Order of accuracy via the rescaled symbols

In general, it is difficult to assess the accuracy of finite different schemes for nonlocal operators, precisely because the nonlocality prevents conventional approaches using Taylor expansions. Nevertheless, under modest conditions on the decay of the underlying functions in Fourier space, the order of accuracy of the scheme (FLh) can be computed formally, that is,

$$(-\Delta)^{\alpha/2}u(x_j) - (-\Delta_h)^{\alpha/2}u_j = \frac{1}{2\pi} \left[ \int_{-\infty}^{\infty} |\xi|^\alpha e^{i\xi x_j} \hat{u}(\xi) d\xi - \int_{-\pi/h}^{\pi/h} \tilde{M}_h(\xi) e^{i\xi x_j} \hat{u}(\xi) d\xi \right].$$

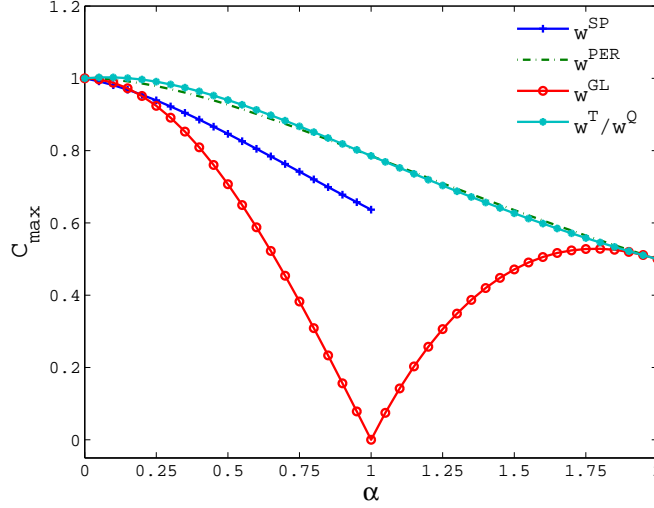


Figure 5.2: The CFL condition  $C_{\max} = (h^\alpha \sum_{k \neq 0} w_k)^{-1} = (-h^\alpha w_0)^{-1}$  for different schemes. The spectral weights  $w^{SP}$  is only plotted for  $\alpha \in (0, 1)$ , as the weights become negative for  $\alpha(1, 2)$ .

If  $\hat{u}(\xi)$  decays to zero fast enough, then the first integral above is essentially determined on the interval  $[-\pi/h, \pi/h]$ , or

$$(-\Delta)^{\alpha/2} u(x_j) - (-\Delta_h)^{\alpha/2} u_j \approx \frac{1}{2\pi} \int_{-\pi/h}^{\pi/h} (|\xi|^\alpha - \tilde{M}_h(\xi)) e^{i\xi x_j} \hat{u}(\xi) d\xi.$$

If the rescaled symbol can be expanded as  $M(\xi) = |\xi|^\alpha (1 + a_1 \xi + a_2 \xi^2 + \dots)$  near the origin, or equivalently  $\tilde{M}_h(\xi) = |\xi|^\alpha (1 + a_1 \xi^2 h^2 + a_2 \xi^2 h^2 + \dots)$ , the above error becomes

$$(-\Delta)^{\alpha/2} u(x_j) - (-\Delta_h)^{\alpha/2} u_j \approx C_1 h + C_2 h^2 + C_3 h^3 + \dots,$$

where the constants

$$C_1 = -\frac{a_1}{2\pi} \int_{-\pi/h}^{\pi/h} \xi |\xi|^\alpha e^{i\xi x_j} \hat{u}(\xi) d\xi, \quad C_2 = -\frac{a_2}{2\pi} \int_{-\pi/h}^{\pi/h} |\xi|^{\alpha+2} e^{i\xi x_j} \hat{u}(\xi) d\xi, \quad \dots$$

are bounded. If  $a_k$  (hence  $C_k$ ) is the first non-zero coefficient in the above expansion of  $M(\xi)$ , the lead order error is  $O(h^k)$ , which is the order of accuracy of the scheme.

Now we can examine the order of accuracy from  $M(\xi)$ . Since  $M^{SP}(\xi)$  is exactly  $|\xi|^\alpha$ , the scheme is spectrally accurate and the error is exactly the integral  $\int_{|\xi| > \pi/h} |\xi|^\alpha e^{i\xi x_j} \hat{u}(\xi) d\xi$ .

For the regularized symbol  $M^{SP}(\xi) = [2(1 - \cos(\xi))]^{\alpha/2}$ , the expansion

$$M^{PER}(\xi) = |\xi|^\alpha \left( 1 - \frac{\alpha}{24} \xi^2 + \left[ \frac{\alpha^2}{1152} - \frac{\alpha}{2880} \right] \xi^4 + \dots \right),$$

implies second order accuracy. For  $M^{GL}(\xi)$  motivated from fractional derivatives, from the simplified expression (26), we have

$$M^{GL}(\xi) = \begin{cases} |\xi|^\alpha \left[ 1 + \frac{\alpha}{2} \tan\left(\frac{\pi\alpha}{2}\right) |\xi| - \left(\frac{\alpha^2}{8} + \frac{\alpha}{12}\right) \xi^2 + \dots \right], & \alpha \in (0, 1) \\ |\xi|^\alpha \left[ 1 + \left(\frac{\alpha}{2} - 1\right) \tan\left(\frac{\alpha\pi}{2}\right) |\xi| - \left(\frac{\alpha^2}{8} - \frac{5\alpha}{12} + \frac{1}{2}\right) \xi^2 + \dots \right], & \alpha \in (1, 2), \end{cases}$$

which implies only first order accuracy. Finally for the weights  $w^T$  or  $w^Q$  from quadrature, although no explicit symbol  $M(\xi)$  available, the accuracy is proved in [27] to be  $h^{2-\alpha}$  for  $w^T$  and  $h^{3-\alpha}$  for  $w^Q$  (seems  $h^{4-\alpha}$  for  $\alpha$  between 1 and 2). The accuracy of these schemes are verified in Figure 5.3, for the fractional Laplacian of  $u(x) = e^{-x^2}$  at the origin, while the spectral convergence of  $w^{SP}$  is already confirmed in Figure 4.2.

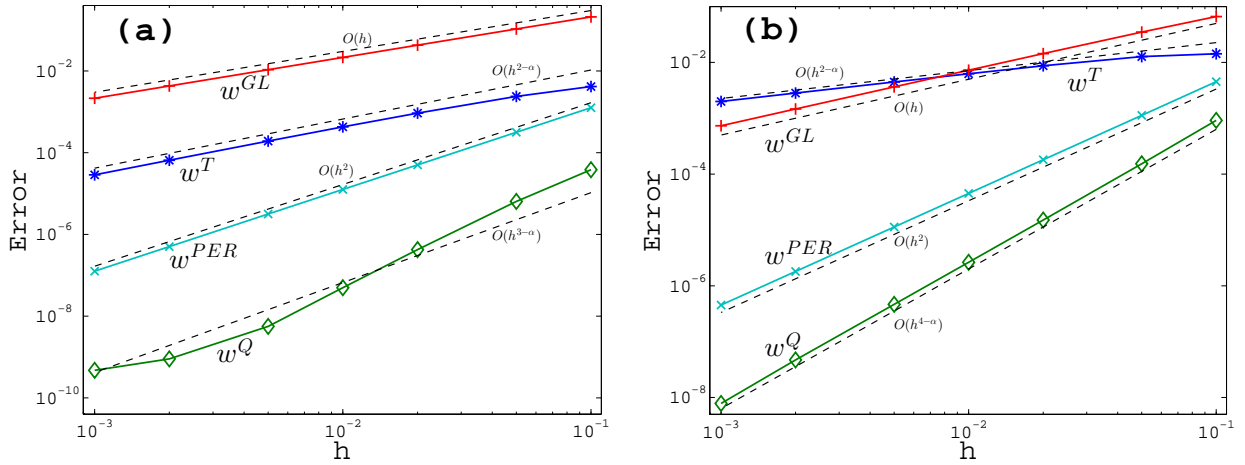


Figure 5.3: Convergence rates of different weights in the scheme (FLh) for the fractional Laplacian of  $u(x) = e^{-x^2}$  at the origin: (a)  $\alpha = 0.8$  and (b)  $\alpha = 1.5$ .

*Remark.* In practice, the discretisation error depends on other factors. If  $u$  is not smooth enough,  $\hat{u}(\xi)$  does not decay to zero fast enough. As a result, the error may be dominated by the integral  $\int_{|\xi| > \pi/h} |\xi|^\alpha e^{i\xi x_j} \hat{u}(\xi) d\xi$ , exhibiting a different rate of convergence. Moreover, when the infinite sum in the scheme (FLh) is truncated, the desired accuracy may be lost due to inappropriate treatment of the boundary conditions.

### 5.3 Summary on the properties of the schemes

Now we can summarise the properties of different schemes, as shown in Table 5.1, and provide some guidance on the right one to implement in practice. The Grünwald-Letnikov scheme, despite its popularity due to the connection with fractional derivatives, has only linear convergence rate and the time step in explicit method for evolution equations could be very restricted at  $\alpha \approx 1$ . The weight  $w^T$  from quadrature with piecewise linear functions has an order of accuracy less than linear for  $\alpha > 1$ . Therefore,  $w^{GL}$  and  $w^T$  are less favoured than the rest schemes. In contrast, both the schemes with  $w^{PER}$  and  $w^Q$  are accurate in most

	Non-negativity	CFL Condition ( $C_{\max}$ )	Accuracy	limit as $\alpha \rightarrow 2^-$
$w^{SP}$	for $0 < \alpha \leq 1$	$\pi^{-\alpha}(1 + \alpha)$	Spectral	No
$w^{PER}$	Yes	$\frac{\alpha\Gamma(\alpha/2)^2}{4\Gamma(\alpha)}$	$O(h^2)$	Yes
$w^{GL}$	Yes	$\cos(\alpha\pi/2), \quad \alpha \in (0, 1)$ $-\cos(\alpha\pi/2)/\alpha, \quad \alpha \in (1, 2)$	$O(h)$	Yes
$w^T$	Yes	$\frac{\pi^{1/2}\Gamma(2 - \alpha/2)}{2^\alpha\Gamma(\frac{1+\alpha}{2})}$	$O(h^{2-\alpha})$	Yes
$w^Q$	Yes	$\frac{\pi^{1/2}\Gamma(2 - \alpha/2)}{2^\alpha\Gamma(\frac{1+\alpha}{2})}$	$O(h^{3-\alpha})$	Yes

Table 5.1: A summary of properties of the weights: the non-negativity (except  $w_0$ ), the CFL condition  $C_{\max} = (-h^\alpha w_0)^{-1}$ , the order of accuracy and the convergence to the three-point standard scheme as  $\alpha \rightarrow 2^-$ .

applications, with all the desired properties. Finally, the spectral method with  $w^{SP}$  is very accurate for smooth and fast decaying functions. However the corresponding weights can be negative for  $\alpha > 1$  and do not reduce to the three-point central difference when  $\alpha$  goes to 2. Therefore, this spectral scheme with  $w^{SP}$  may not always be the best choice.

## 6 Truncation of the far-field boundary conditions

The general scheme (FLh) involves infinitely many terms, which has to be truncated in practice. For Dirichlet problems on a bounded domain, the infinite sum can usually be approximated using the given boundary conditions on the exterior of the domain. For problems posed on the whole space, with zero or other reasonable boundary conditions at infinity, the situation is more complicated, as a result of the slow decay of the solutions commonly observed in various applications. For example, in contrast to compactly supported solutions of the classical porous medium equation  $u_t - \Delta u^m = 0$  for  $m > 1$ , the solutions of the fractional porous medium equation  $u_t + (-\Delta)^{\alpha/2} u^m = 0$  in  $\mathbb{R}^n$  has an algebraic tail of order  $|x|^{-N-\alpha}$  for  $\alpha \in (0, 2)$ , as shown in [54]. Because of this slow decay to zero, a straightforward truncation like  $\sum_{k=-M}^M (u_j - u_k) w_{j-k}$  of (FLh) may lead to significant errors even for relative large value of  $M$ .

A first step towards truncating the asymptotic far-field boundary condition was given by the authors in [27], and is reviewed briefly below. Without loss of generality, the computational domain is denoted by  $[-L, L]$ , on which the fractional Laplacian of  $u$  at  $x_j$  is sought.

To proceed, first the singular integral (2) is decomposed into three parts,

$$\begin{aligned}
(-\Delta)^{\alpha/2}u(x_j) &= \underbrace{C_{1,\alpha} \int_{-L_M}^{L_M} (u(x_j) - u(y))|x_j - y|^{-1-\alpha} dy}_{\text{(I)}} \\
&\quad + \underbrace{C_{1,\alpha}u(x_j) \int_{|y|>L_M} |x_j - y|^{-1-\alpha} dy}_{\text{(II)}} - \underbrace{C_{1,\alpha} \int_{|y|>L_M} u(y)|x_j - y|^{-1-\alpha} dy}_{\text{(III)}}, \quad (27)
\end{aligned}$$

for some  $L_M \geq L$ . The first term (I) is approximated by the finite truncation  $\sum_{k=-M}^M (u_j - u_k)w_{j-k}$ , and the integral in the second term (II) can be evaluated exactly, while the last term (III) has to be estimated using asymptotic far-field boundary conditions. If  $u$  decays to zero with an algebraic rate  $\beta$ , that is  $u(x) = O(|x|^{-\beta})$  for some  $\beta > 0$ , then

$$u(y) \approx u(\pm L)L^\beta|y|^{-\beta}, \quad y \rightarrow \pm\infty. \quad (28)$$

Hence the last term (III) can be estimated using the following two integrals,

$$\begin{aligned}
C_{1,\alpha} \int_{L_M}^{\infty} u(y)|x_j - y|^{-1-\alpha} dy &\approx C_{1,\alpha}u(L)L^\beta \int_{L_M}^{\infty} (y - x_j)^{-1-\alpha}y^{-\beta} dy \\
&= \frac{C_{1,\alpha}u(L)L^\beta}{(\alpha + \beta)(L_M)^{\alpha+\beta}} {}_2F_1\left(\alpha + 1, \alpha + \beta; \alpha + \beta + 1; \frac{x_j}{L_M}\right), \quad (29)
\end{aligned}$$

and

$$\begin{aligned}
C_{1,\alpha} \int_{-\infty}^{-L_M} u(y)|x_j - y|^{-1-\alpha} dy &\approx C_{1,\alpha}u(-L)L^\beta \int_{-\infty}^{-L_M} (x_j - y)^{-1-\alpha}(-y)^{-\beta} dy \\
&= \frac{C_{1,\alpha}u(-L)L^\beta}{(\alpha + \beta)(L_M)^{\alpha+\beta}} {}_2F_1\left(\alpha + 1, \alpha + \beta; \alpha + \beta + 1; -\frac{x_j}{L_M}\right), \quad (30)
\end{aligned}$$

in terms of the Gauss hypergeometric function  ${}_2F_1$ .

*Remark.* We add a few more comments related to the practical implementation of this approach. If the exact value of the exponent  $\beta$  is not available from existing theory, it can still be estimated from the solution itself by fitting the computed data. The extended domain size  $L_M$  should be strictly larger than  $L$  ( $L_M = 3L$  in [27]), to avoid any possible singularity of  ${}_2F_1(\alpha + 1, \alpha + \beta; \alpha + \beta + 1; z)$  at  $z = 1$ . In this way, if  $x_k$  is outside the interval  $[-L, L]$ ,  $u_k$  can be approximated by (28) in the computation of the finite sum  $\sum_{k=-M}^M (u_j - u_k)w_{j-k}$ .

The above treatment of the far-field boundary condition is natural in the context of the difference-quadrature scheme derived in [27], based on the singular integral (2). It turns out that the same approach works for a wide variety of schemes, because of the ubiquitous scaling  $w_k \approx C_{1,\alpha}h^{-\alpha}k^{-1-\alpha}$  shared by most of the weights (see Section 5.1). This scaling behaviour is expected from a careful comparison between the singular integral (2) and the scheme (FLh), that is,

$$w_k \approx C_{1,\alpha} \int_{x_k-h/2}^{x_k+h/2} |y|^{-1-\alpha} dy \approx C_{1,\alpha} \int_{x_k-h/2}^{x_k+h/2} |x_k|^{-1-\alpha} dy = C_{1,\alpha}h^{-\alpha}k^{-1-\alpha}.$$

Therefore, if  $u(y)$  is approximated by the constant  $u(x_k)$  for  $y \in (x_k - h/2, x_k + h/2)$ ,

$$(u_j - u_k)w_{j-k} \approx C_{1,\alpha} \int_{x_k-h/2}^{x_k+h/2} |x_j - y|^{-1-\alpha} (u(x_j) - u(y)) dy, \quad (31)$$

and the infinite sum in the scheme (FLh) can be written as

$$\begin{aligned} \sum_{k=-M}^M (u_j - u_k)w_{j-k} + \sum_{k>|M|} (u_j - u_k)w_{j-k} &\approx \sum_{k=-M}^M (u_j - u_k)w_{j-k} \\ &+ C_{1,\alpha} u_j \int_{|y|>x_M+h/2} |x_j - y|^{-1-\alpha} dy - C_{1,\alpha} \int_{|y|>x_M+h/2} u(y)|x_j - y|^{-1-\alpha} dy. \end{aligned} \quad (32)$$

Since the last two integrals are exactly the same as those in (27) with  $L_M = x_M + h/2$ , the far-field boundary conditions with other weights can be handled in the same way as that in [27].

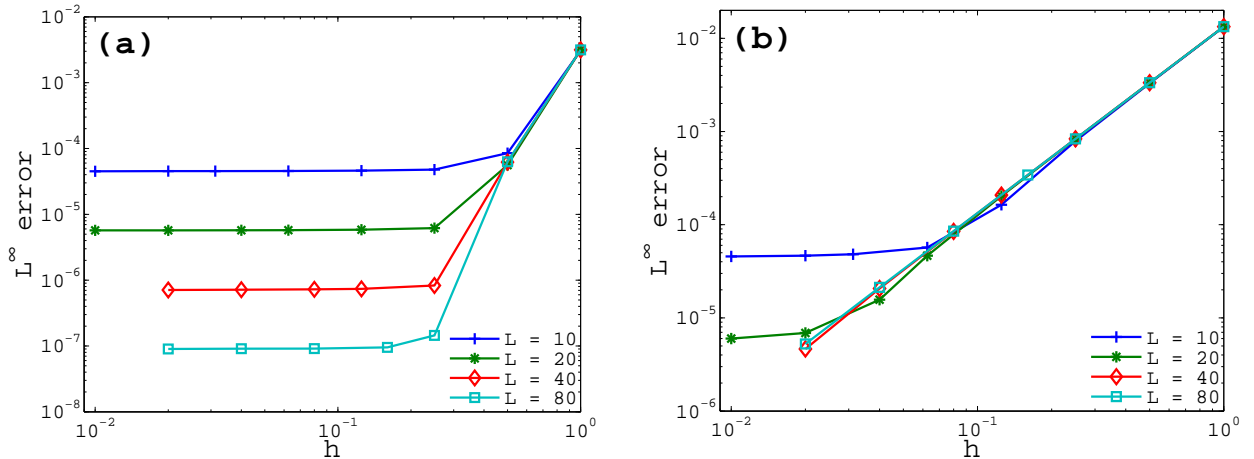


Figure 6.1: The  $L^\infty$  error of the fractional Laplacian of  $u(x) = (1 + x^2)^{-(1-\alpha)/2}$  with  $\alpha = 0.4$  using the approximation (32): (a) the spectral weights  $w^{SP}$ ; (b) the weights  $w^{PER}$ .

The effectiveness of this the far-field boundary condition is shown in Figure 6.1 on different domain sizes  $L$  and grid sizes  $h$ , for the function  $u(x) = (1 + x^2)^{-(1-\alpha)/2}$  and its Fractional Laplacian

$$(-\Delta)^{\alpha/2} u(x) = 2^\alpha \Gamma\left(\frac{1+\alpha}{2}\right) \Gamma\left(\frac{1-\alpha}{2}\right)^{-1} (1+x^2)^{-(1+\alpha)/2}. \quad (33)$$

The convergence rates for  $w^{SP}$  and  $w^{PER}$  shown in Figure 6.1 are very similar to those in [27] for  $w^Q$ : as the grid size  $h$  decreases, the error decreases with the expected rate as summarized in Table 5.1, then it levels off because its dominant contribution is taken over by the boundary condition.

*Remark.* The error for  $w^{SP}$  seems to be “spectral” before saturation, when  $\alpha$  is between 0 and 1 as in Figure 6.1. However when  $\alpha$  is between 1 and 2,  $w_k^{SP}$  scales like  $k^{-2}h^{-\alpha}$

with alternating signs. The approximation (31) is no longer valid (at least with respect to the expected accuracy), and the above approach to the far-field boundary condition is less effective for  $w^{SP}$ .

## 7 Convergence for equations with fractional Laplacian operators

Although the efficient and accurate evaluation of the fractional Laplacian is fundamental, its practical applications in the numerical solutions of equations with this operator are equally important. In this section, we study the convergence of the canonical extended Dirichlet boundary value problem,

$$\begin{aligned} (-\Delta)^{\alpha/2}u &= f & \text{for } x \in D, \\ u &= g & \text{for } x \in \mathbb{R}^n \setminus D. \end{aligned} \tag{FLD}$$

Here  $D$  is a bounded domain on which the unknown function  $u$  is sought and  $g$  is the boundary condition. The problem (FLD) is the analogue of the Dirichlet problem for the Laplace operator, except that, here  $g$  is given on the complement of the domain  $D$ , instead of just the boundary  $\partial D$ . In the special case  $g = 0$ ,  $f = 1$ , the solution  $u$  corresponds to the expected first passage time (or mean exit time) of the symmetric  $\alpha$ -stable Lévy process from a given domain [20]. When the domain  $D$  is a ball about the origin and  $f = 0$ , the solution can be written explicitly as a potential integral of  $g$  (see [35, Chapter I] and [47, Section 5.1] for more details), extending the Poisson formula for the Laplace equation to the fractional setting.

Consider (FLD) in one dimension with  $D = (-1, 1)$ . When the scheme (FLh) is applied, the discrete problem becomes

$$\begin{aligned} (-\Delta_h)^{\alpha/2}u_j &= f_j & \text{for } j \in D_h, \\ u_j &= g_j & \text{for } j \in D_h^C, \end{aligned} \tag{FLD}_h$$

where  $D_h = \{j \in \mathbb{Z} : |jh| < 1\}$ ,  $D_h^C = \mathbb{Z}_h \setminus D_h$  with  $f_j = f(x_j)$  and  $g_j = g(x_j)$ . We are interested in the convergence of the numerical solution  $u_j$  to the exact solution  $u(x_j)$  on  $D_h$ , as the grid size  $h$  decreases. When different weights are employed in the discrete operator  $(-\Delta_h)^{\alpha/2}$ , an order  $O(h^p)$  local truncation error of the residue  $r_j = (-\Delta_h)^{\alpha/2}u(x_j) - f(x_j)$  does not always imply the same order of error  $e_j = u(x_j) - u_j$  for the numerical solution; some form of stability is required. In terms of the errors  $r_j$  and  $e_j$ , the discrete problem (FLD)<sub>h</sub> becomes

$$(-\Delta_h)^{\alpha/2}e_j = r_j \quad \text{for } j \in D_h, \quad e_j = 0 \quad \text{for } j \in D_h^C. \tag{34}$$

This can be written as a linear algebra problem  $L_h \mathbf{e}_h = \mathbf{r}_h$ , for some matrix  $L_h$ , vectors  $\mathbf{e}_h$  denoting the numerical error  $e_j$  with  $j \in D_h$  and  $\mathbf{r}_h$  denoting the consistency error  $r_j$ . The stability (or the equivalence of the two errors) is essentially the boundedness of the inverse matrix  $(L_h)^{-1}$  in suitable norms.

In many cases, the norm  $\|(L_h)^{-1}\|$  is difficult to estimate, as the entries of the matrix  $L_h$  depend on the particular weights in the discretization. Alternatively, the same stability conditions can be established by constructing discrete supersolutions and applying the discrete



maximum principle, in a similar way as for classical elliptic equations [36]. To process, we have the following lemma.

*Lemma 7.1* (Discrete maximum principle). Let  $u$  defined on  $\mathbb{Z}_h$  satisfy  $(-\Delta_h)^{\alpha/2}u_j \leq 0$  for  $j \in D_h$ , for any discretization (FLh) with nonnegative weights  $w_k$  for  $k \neq 0$ . Then

$$\max_{j \in D_h} u_j \leq \max_{j \in D_h^C} u_j.$$

Similarly, if  $(-\Delta_h)^{\alpha/2}u_j \geq 0$  for  $j \in D_h$ , then

$$\min_{j \in D_h} u_j \geq \min_{j \in D_h^C} u_j.$$

Next we would like to construct discrete supersolutions  $v$  on  $\mathbb{Z}_h$ , which satisfies

$$\begin{aligned} (-\Delta_h)^{\alpha/2}v_j &\geq 1, & \text{for } j \in D_h, \\ v_j &\geq 0, & \text{for } j \in D_h^C. \end{aligned} \tag{35}$$

Applying Lemma 7.1,  $v$  is automatically non-negative on  $D_h$ . If such a supersolution  $v$  exists on  $\mathbb{Z}_h$ , the discrete function  $p$  defined as  $p_j = \|\mathbf{r}_h\|_{\infty}v_j \pm e_j$  satisfies  $(-\Delta_h)^{\alpha/2}p_j \geq 0$  for  $j \in D_h$  and  $p_j \geq 0$  for  $j \in D_h^C$ . Therefore,  $p$  is non-negative on  $\mathbb{Z}_h$ , and the numerical error  $|e_j|$  is bounded by  $\|\mathbf{r}_h\|_{\infty}\|v\|_{\infty}$ , showing the same order of local truncation error  $\mathbf{r}_h$  and numerical error  $\mathbf{e}_h$ . For classical elliptic equations, the supersolutions (either continuous or discrete) can usually be chosen as an inverted parabola, but it is more difficult for the equations with the fractional Laplacian. In [27], the following discrete supersolution

$$v_j = \begin{cases} 4 - (jh)^2, & |jh| < 1 \\ 0, & \text{otherwise,} \end{cases}$$

is chosen (associated with the weights  $w^Q$ ), and the conditions (35) is verified with some technical assumptions. When other weights are used in the scheme (FLh), (35) may be difficult to verify analytically for a specific choice of supersolutions. Instead, we look for motivation from the continuous supersolution  $v_G$ , which satisfies

$$(-\Delta)^{\alpha/2}v_G(x) = 1, \quad x \in (-1, 1),$$

and  $v_G(x) \equiv 0$  for  $|x| \geq 1$ , by showing numerically that  $v_{Gj} = v_G(x_j)$  is a discrete supersolution. This function  $v_G$  is the first passage time from the unit ball for particles under symmetric  $\alpha$ -stable process [20] and is explicitly given by

$$v_G(x) = K_{\alpha}(1 - |x|^2)_+^{\alpha/2}, \quad K_{\alpha} = \frac{2^{\alpha}}{\sqrt{\pi}}\Gamma\left(1 + \frac{\alpha}{2}\right)\Gamma\left(\frac{1 + \alpha}{2}\right).$$

The discrete fractional Laplacian of  $v_G$  is shown in Figure 7.1 for various scheme with  $\alpha = 0.5$  and  $\alpha = 1.5$ . It seems that (35) is always satisfied, and  $v_G$  is a valid supersolution with the associated weights <sup>2</sup>.

<sup>2</sup> It is important to make sure that the boundary  $\pm 1$  lies also on the boundary  $\partial D_h^C$ , i.e.,  $1/h$  is an integer.

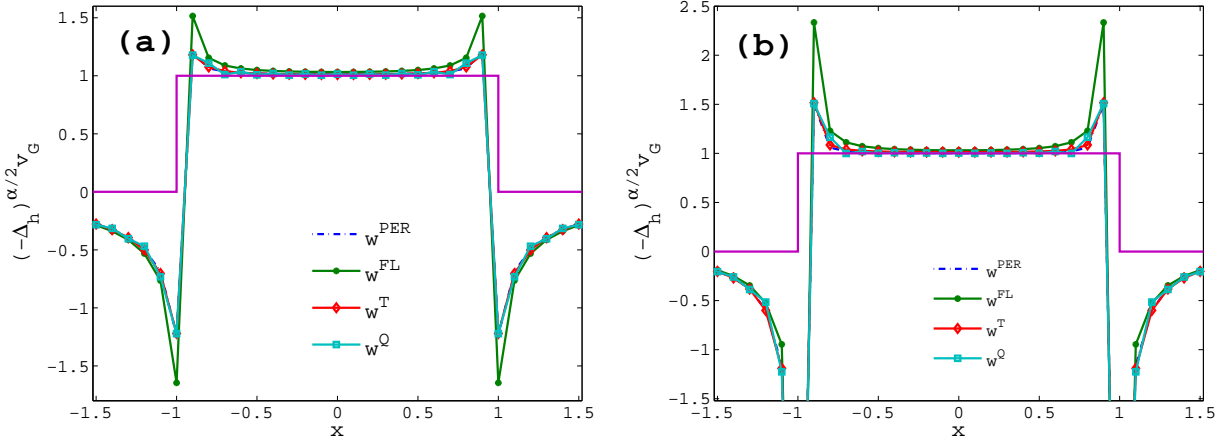


Figure 7.1: The (discrete) fractional Laplacian of  $v_G$  for various schemes: (a)  $\alpha = 0.5$  and (b)  $\alpha = 1.5$ , suggesting that  $v_G$  is a discrete supersolution for all  $\alpha \in (0, 2)$  and all non-negative weights considered in this paper.

## 8 Numerical experiments and applications to nonlinear PDEs

In this section, we provide several numerical examples, to further verify the accuracy of the scheme with different weights, especially the relation between the order of convergence and the regularity of the functions, and to showcase the applications in various PDEs.

### 8.1 Accuracy when the solutions are non-smooth

The order of accuracy of the schemes derived in Section 5.2 is valid only for smooth functions, such that the integral  $\int_{|\xi| > \pi/h} |\xi|^\alpha e^{i\xi x_j} \hat{u}(\xi) dx$  can be safely ignored. For less smooth functions, the actual convergence rate can be lower as we show now. The examples used in this and the next subsection re related to the following result [5, 26]

$$(-\Delta)^{\frac{\alpha}{2}} (1-x^2)_+^{k+\frac{\alpha}{2}} = \begin{cases} K_{k,\alpha} {}_2F_1\left(\frac{1+\alpha}{2}, -k; \frac{1}{2}; x^2\right), & |x| < 1, \\ \tilde{K}_{k,\alpha} {}_2F_1\left(\frac{1+\alpha}{2}, \frac{2+\alpha}{2}; \frac{3+\alpha}{2} + k; \frac{1}{x^2}\right), & |x| > 1, \end{cases} \quad (36)$$

where  $k$  is an integer,

$$K_{k,\alpha} = \frac{2^\alpha \Gamma(k+1+\frac{\alpha}{2}) \Gamma(\frac{1+\alpha}{2})}{k! \Gamma(\frac{1}{2})}, \quad \tilde{K}_{k,\alpha} = \frac{2^\alpha \Gamma(k+1+\frac{\alpha}{2}) \Gamma(\frac{1+\alpha}{2})}{\Gamma(-\frac{\alpha}{2}) \Gamma(\frac{3+\alpha}{2} + k)},$$

and  ${}_2F_1$  is the Gauss hypergeometric function [1]. Since  $(1-x^2)_+^{k+\frac{\alpha}{2}}$  is supported on the interval  $[-1, 1]$  for any  $k \geq 0$  and  $\alpha \in (0, 2)$ , the sum in the scheme (FLh) has only finite number of terms and can be truncated appropriately.

The fractional Laplacian of  $u(x) = (1-x^2)_+^{2+\alpha/2}$  is computed with different weights, and the results with a grid size  $h = 0.2$  and the converge rates are shown in Figure 8.1. While

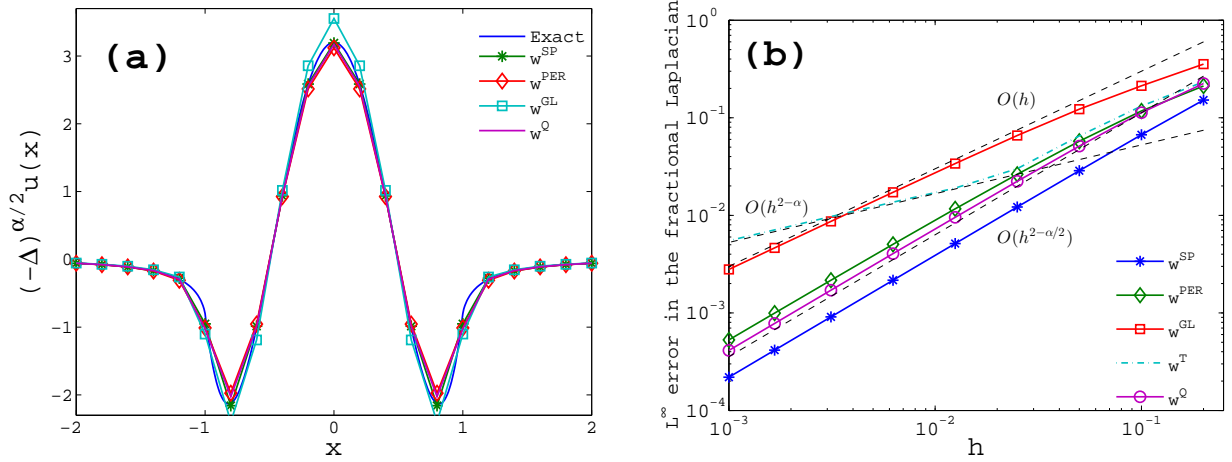


Figure 8.1: The fractional Laplacian of  $u(x) = (1 - x^2)_+^{2+\alpha/2}$  with  $\alpha = 1.5$ : **(a)** the result a grid with spacing  $h = 0.2$ ; **(b)** the order of convergence (measured in  $L^\infty$  norm) with different  $h$ .

lower order schemes with weights  $w^{GL}$  and  $w^T$  exhibit the expected order of convergence derived in Section 5.2, higher order schemes with other weights have the same less optimal convergence rate  $O(h^{2-\alpha/2})$ . This rate can be explained from the asymptotic expansion of  $\int_{|\xi|>\pi/h} |\xi|^\alpha e^{i\xi x_j} \hat{u}(\xi) d\xi$ , the source of the dominant error. In fact, the Fourier transform of  $u(x) = (1 - x^2)_+^{k+\alpha/2}$  can be explicitly expressed as

$$\hat{u}(\xi) = \int_{-\infty}^{\infty} (1 - x^2)_+^{k+\alpha/2} e^{-ix\xi} dx = F_{k,\alpha} |\xi|^{-k-(\alpha+1)/2} J_{k+(\alpha+1)/2}(|\xi|),$$

in terms of the Bessel function  $J_\nu$  and the constant factor

$$F_{k,\alpha} = \sqrt{\pi} \Gamma\left(k + 1 + \frac{\alpha}{2}\right) 2^{k+(\alpha+1)/2}.$$

At  $x_j = 0$ , the integral  $\int_{|\xi|>\pi/h} |\xi|^\alpha e^{i\xi x_j} \hat{u}(\xi) d\xi$  is bounded by

$$F_{k,\alpha} \int_{|\xi|>\pi/h} |\xi|^{-k+(\alpha-1)/2} |J_{k+(\alpha+1)/2}(|\xi|)| dx \sim \int_{|\xi|>\pi/h} |\xi|^{-k+\alpha/2-1} d\xi = O(h^{k-\alpha/2}),$$

using asymptotic form  $J_\mu(|\xi|) \sim \sqrt{\frac{2}{\pi|\xi|}} \cos(|\xi| - \frac{\alpha\pi}{2} - \frac{\pi}{4})$  as  $|\xi|$  goes to infinity. The dominant order  $O(h^{2-\alpha/2})$  error in Figure 8.1(b) corresponds to the choice  $k = 2$  in the function  $u(x) = (1 - x^2)_+^{2+\alpha/2}$ . As a general rule, if a function  $u$  is in Hölder space  $C^{k,\beta}$  with optimal exponent  $\beta$ , then its discrete fractional Laplacian  $(-\Delta)^{\alpha/2}u$  has an order of accuracy at most  $k + \beta - \alpha$ .

## 8.2 The extended Dirichlet problem

We now check the accuracy of the scheme when it is applied to the extended Dirichlet problem (FLD), by choosing  $D = (-1, 1)$ ,  $f(x) = K_{k,\alpha} {}_2F_1\left(\frac{1+\alpha}{2}, -k; \frac{1}{2}; x^2\right)$  on  $D$  and  $g \equiv 0$

on  $D^C$ . From (36), the exact solution is  $u(x) = (1 - x^2)_+^{k+\alpha/2}$ . The convergence rates with various weights are shown in Figure 8.2, for  $k = 1$  and  $k = 3$  respectively. Because the solution is not smooth near the boundary  $x = \pm 1$ , the order of accuracy could be lower than the theoretical one. In general, if the solution is in the Hölder space  $C^{k,\beta}$  with optimal exponent  $\beta$ , then the optimal order of convergence is  $k + \beta$ , even if a more accuracy scheme is used.

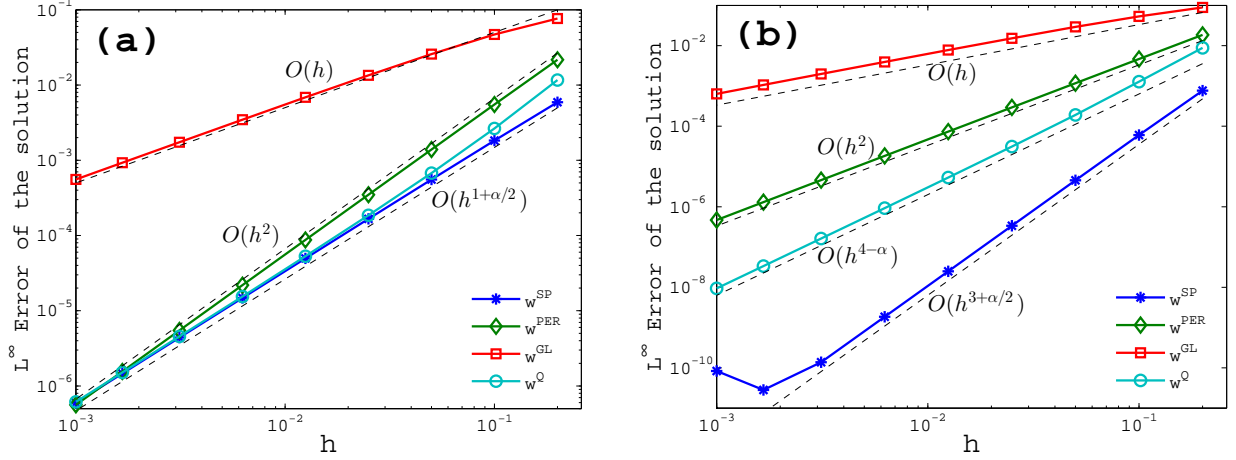


Figure 8.2: The convergence of the solution (measured in  $L^\infty$  error) for the extended Dirichlet problem (FLD) corresponding to the relation (36) (with  $\alpha = 1.5$ ): (a)  $k = 1$  and (b)  $k = 3$ . Because of the non-smoothness of the solution, the order of accuracy is at most  $k + \alpha/2$ , even for higher order schemes.

### 8.3 Fractional heat equation

We now move to the numerical solutions of evolution equations with the fractional Laplacian operator, starting from the simplest fractional heat equation

$$u_t + (-\Delta)^{\alpha/2}u = 0, \quad u(x, 0) = u_0(x). \quad (37)$$

Here  $u$  is usually the probability distribution function of particles undergoing  $\alpha$ -stable processes, analogous to that in the heat equation governed by Brownian motion. The solution to (37) can also be explicitly written as

$$u(x, t) = \int_{\mathbb{R}^n} G_\alpha(x - y, t)u_0(y)dy,$$

where  $G_\alpha(x, t)$  is the Green's function with Fourier transform  $\hat{G}_\alpha(k, t) = \exp(-|\xi|^{\alpha t})$ .

Starting from the sign function  $u_0(x) = \text{sign}(x)$ , the solution at  $t = 0.5$  is shown in Figure 8.3, for  $\alpha = 0.5$  and  $\alpha = 1.5$ , respectively. The solution is computed with weight  $w^{PER}$  on the domain  $[-10, 10]$ , with grid size  $h = 0.1$  and time step  $\Delta t = 0.01$  (for  $\alpha = 0.5$ ) and  $\Delta t = 0.0032$  (for  $\alpha = 1.5$ ). The treatment of the far field boundary conditions  $u(\pm\infty) = \pm 1$

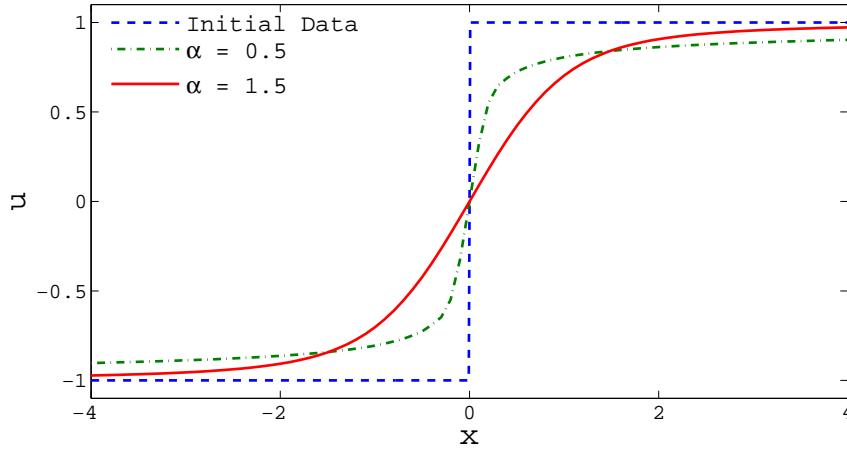


Figure 8.3: The spreading of the sign function under fractional diffusion equation (37) at time  $t = 0.5$ , for  $\alpha = 0.5$  and  $\alpha = 1.5$  respectively.

is adapted from that in Section 6, using the fact that  $u(x) \pm 1 \sim |x|^{-\alpha}$  as  $x \rightarrow \pm\infty$ . While both solutions spread in space, the larger  $\alpha$  is, the smoother the solution becomes near its initial discontinuity, and the closer the solution stays to its boundary condition.

## 8.4 Fractal Burgers Equation

In this subsection, several numerical solutions of the fractional Burgers equation [4, 52]

$$u_t + \partial_x \left( \frac{u^2}{2} \right) + \kappa (-\partial_{xx})^{\alpha/2} u = 0 \quad (38)$$

are demonstrated. This equation (often called fractal Burgers equation in literature) is one of the most well-studied conservation laws with fractional Laplacian [4]. Many properties shared by general fractional conservation laws can be understood through this simple equation. Depending on the initial data and the exponent  $\alpha$ , general behaviours of solutions to (38) are different. For increasing initial data with constant far field (say zero), the long time asymptotics is described by the inviscid Burgers equation for  $\alpha \in (1, 2]$  (see [32]), but is governed by the fractional heat equation for  $\alpha \in (0, 1)$  (see [3]). For decreasing initial data with constant far field and  $\alpha \in (0, 1)$ , the solution can develop shocks under different conditions [2, 4, 17, 33].

Let  $F_{j+1/2}^n$  be the numerical flux corresponding to  $u^2/2$  at space  $x_{j+1/2}$  and time  $t_n$ , then a straightforward explicit discretization of (38) is

$$\frac{u_j^{n+1} - u_j^n}{\Delta t} + \frac{F_{j+1/2}^n - F_{j-1/2}^n}{\Delta x} + \nu \sum_{k=-\infty}^{\infty} (u_j^n - u_k^n) w_{j-k} = 0.$$

For the initial condition  $u_0(x) = \text{sign}(x)$ , the solution is a rarefaction wave in the inviscid case ( $\kappa = 0$ ), and is smoother in the presence of fractional diffusion, as shown in Figure 8.4.

The computation domain is the interval  $[-10, 10]$  with grid size  $h = 0.1$  and time step  $0.1h^\alpha$ , using the weights  $w^{PER}$ . Despite the nonlinear term  $(u^2/2)_x$  in (38), the solution has the same asymptotic far field boundary condition  $u(x) \pm 1 \sim |x|^{-\alpha}$  as  $x \rightarrow \pm\infty$ .

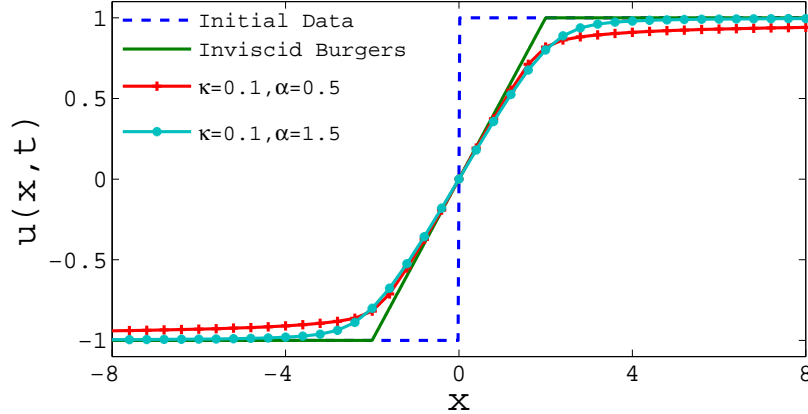


Figure 8.4: The solution to the fractal Burgers equation (38) at  $t = 2$ , compared with the rarefaction wave governed by the inviscid Burgers equation.

When the initial data  $u_0(x) = -\text{sign}(x)$  is chosen,  $u(x, t) = u_0(x)$  is a stationary shock in the inviscid case. When the fractional diffusion is turned on, the solution may become continuous when  $\alpha$  is larger than one (see Figure 8.5) or when the coefficient  $\kappa$  is large enough (see Figure 8.6). Although these numerical evidences are not conclusive for the existence of the shocks, especially when the profile could be poorly resolve, they are consistent with limited existing results [2, 4, 17, 33].

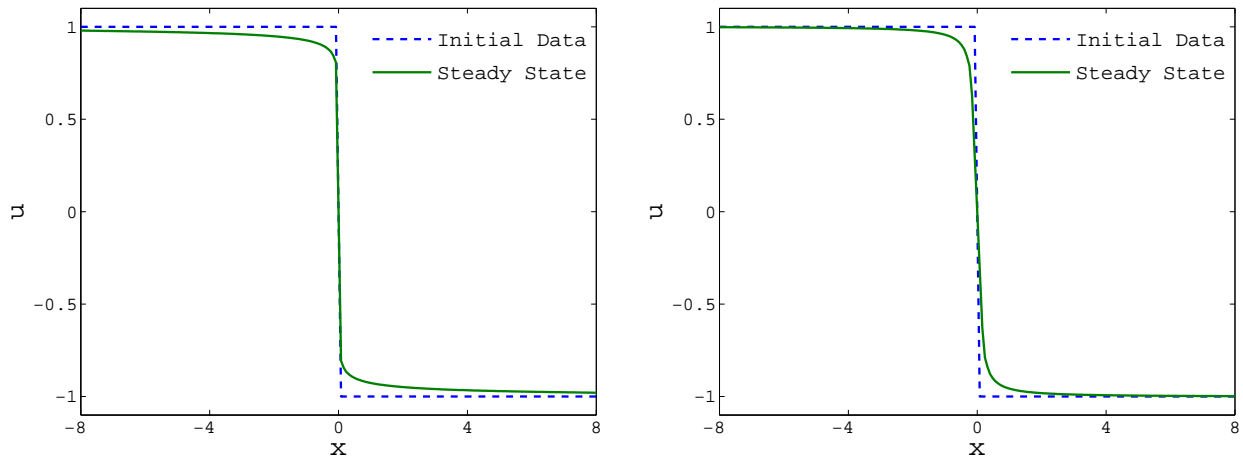


Figure 8.5: The steady state of the fractal Burgers equation (38) ( $\kappa = 1$ ) with initial data  $u_0(x) = -\text{sign}(x)$  for  $\alpha = 0.8$  (left) and  $\alpha = 1.2$  (right), respectively.

For other integrable initial data with zero boundary condition at infinity, similar features like smoothing of negative slopes and steepening of positive slopes are expected. For the

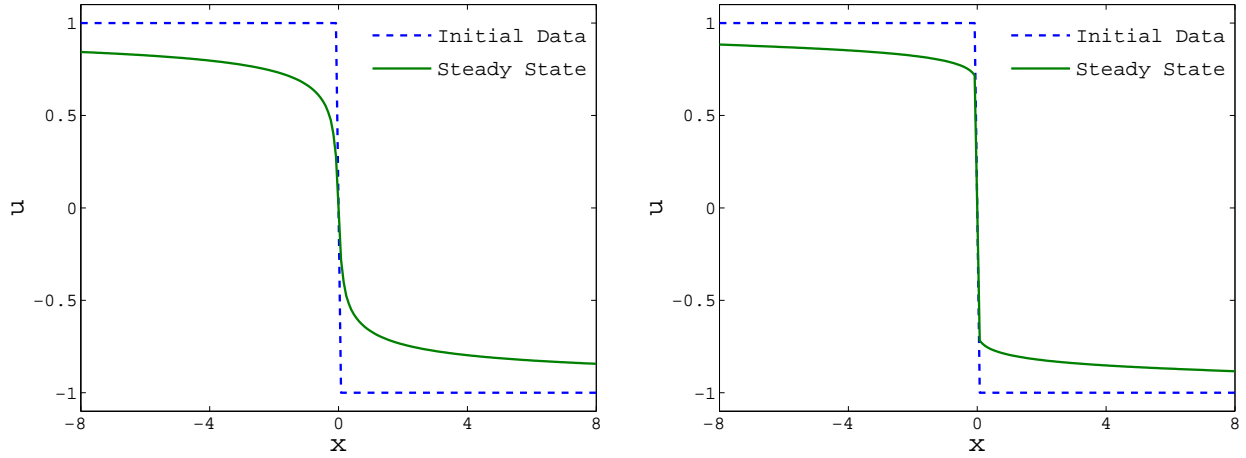


Figure 8.6: The steady state of the fractal Burgers equation (38) ( $\alpha = 0.4$ ) with initial data  $u_0(x) = -\text{sign}(x)$  for  $\kappa = 1.0$  (left) and  $\kappa = 0.1$  (right), respectively. The steady state seems continuous when  $\kappa$  is relatively large but becomes “discontinuous” when  $\kappa$  is small.

initial condition

$$u_0(x) = \begin{cases} \cos x, & |x| \leq \pi/2, \\ 0, & \text{otherwise,} \end{cases} \quad (39)$$

the solutions at  $t = 4$  and  $t = 8$  are shown in Figure 8.7. When  $\alpha < 1$  and  $\kappa$  is small, a discontinuity in the solution is expected [2], although the precise conditions for the occurrence of shocks are yet unknown.

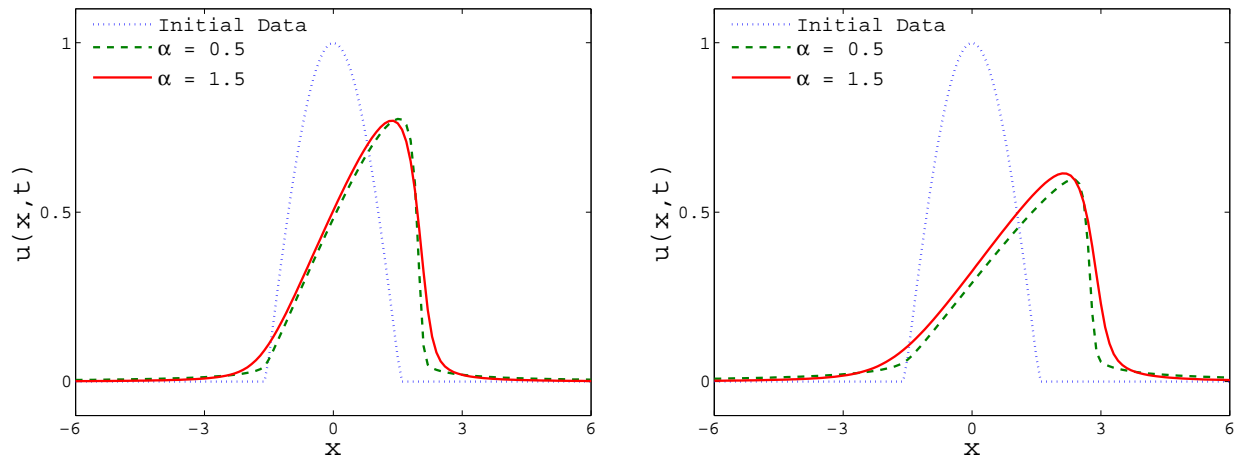


Figure 8.7: The solution of the fractal Burgers equation at  $t = 4$  (left) and  $t = 8$  (right) with initial condition (39).

## 8.5 Fractional thin film equation

The fractional thin film equation  $u_t = \nabla \cdot (u \nabla (-\Delta)^{\alpha/2} u)$  appears in fracture dynamics [28]. Below we focus on the equation in similarity variables, that is,

$$u_t = \nabla \cdot (u \nabla (-\Delta)^{\alpha/2} u) + \lambda \nabla \cdot (xu), \quad (40)$$

which possesses a stationary steady instead of spreading and decaying densities. If we choose  $\lambda = 2(1 + \alpha)C_{1,\alpha}$  and initial data with the total conserved mass

$$M = \int_{\mathbb{R}} u(x, t) dx = \sqrt{\pi} \Gamma \left( 2 + \frac{a}{2} \right) \Gamma \left( \frac{5 + a}{2} \right)^{-1},$$

then it is easy to check that  $u_{\infty}(x) = (1 - x^2)^{1+\alpha/2}$  is the steady state. The time evolution of the solution starting from the initial data

$$u_0(x) = \frac{M}{\sqrt{\pi}} \left( 0.8e^{-4(x-1)^2} + 1.6e^{-16(x+2)^2} \right) \quad (41)$$

is shown in Figure 8.8. Since the solution is essentially supported on an interval, the computational domain  $[-4, 4]$  is chosen, with grid size  $h = 0.01$  and time step  $\Delta t = 0.0001$ . Clearly the steady state  $u_{\infty}(x)$  is approached as time evolves.

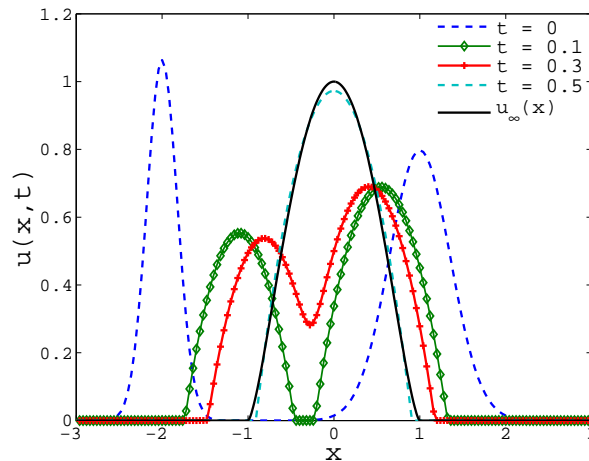


Figure 8.8: The evolution of solutions to (40) start with initial data (41) consisting two Gaussians.

## 9 Conclusions

In this article we performed a comprehensive study of finite difference approximation of the fractional Laplacian operator of the form (FLh). The resulting discrete operator is a multiplier in the spectral space, and the connection between the weights and the rescaled symbol



is established. Many schemes are derived or reviewed in this context, and are compared in various ways about the asymptotic scaling of the weights and their order of accuracy. Other practical issues are also highlighted, like the treatment of the far field boundary conditions and the effect the non-smoothness of the solutions on the resulting accuracy. The schemes can be applied to many PDEs with fractional Laplacian, and provide robust tools for numerical investigation on these more difficult equations besides theoretical analysis.

This numerical scheme can be generalised easily to translation-invariant operator  $\mathcal{L}$  with symbol or multiplier  $\tilde{M}$  in the spectral space. That is,

$$\mathcal{L}u_j = \sum_{k=-\infty}^{\infty} w_k u_{j-k}, \quad (42)$$

such that

$$\tilde{M}_h(\xi) := h \sum_{k=-\infty}^{\infty} w_k e^{-i\xi x_k} \sim \tilde{M}(\xi),$$

near the origin. From a given symbol  $\tilde{M}_h(\xi)$ , the weights are expressed as

$$w_k = \frac{1}{2\pi} \int_{-\pi/h}^{\pi/h} \tilde{M}_h(\xi) e^{i\xi x_k} d\xi.$$

For operators like  $\sqrt{1 - \Delta}$ , the weights  $w_k$  normally depend on the grid size  $h$  in a complicated way, but for scale invariant operators like  $(-\Delta)^{\alpha/2}$  and  $(-\Delta)^{-\alpha/2}$ ,  $h$  can be factored out from the weights, as we did in Section 2.2. Further more, if  $\tilde{M}$  vanishes at the origin, it is reasonable to require that  $\tilde{M}_h(0) = 0$  and the scheme (42) can be written as (FLh).

While the framework of the scheme (FLh) can be extended in a straightforward way into higher dimensions, several practical limitations do appear. Explicit expressions of the weights like (19) and (22) are less likely for any given symbol like  $M(\xi) = (\xi_1^2 + \xi_2^2 + \dots + \xi_n^2)^{\alpha/2}$ . As a result, numerical quadratures of oscillatory integrals are inevitable [30, 29]. The far field boundary conditions are also more difficult to treat. In one dimension, the function only decays in two directions. But the flat tails in higher dimensions, if they exist, are much more complicated. As a result, there are many important future questions to be answered for the fractional Laplacian in particular and for nonlocal equations in general.

## References

- [1] M. Abramowitz and I. A. Stegun, editors. *Handbook of mathematical functions with formulas, graphs, and mathematical tables*. Dover Publications Inc., New York, 1992.
- [2] N. Alibaud, J. Droniou, and J. Vovelle. Occurrence and non-appearance of shocks in fractal Burgers equations. *J. Hyperbolic Differ. Equ.*, 4(3):479–499, 2007.
- [3] N. Alibaud, C. Imbert, and G. Karch. Asymptotic properties of entropy solutions to fractal Burgers equation. *SIAM J. Math. Anal.*, 42(1):354–376, 2010.

- [4] P. Biler, T. Funaki, and W. A. Woyczynski. Fractal Burgers equations. *J. Differential Equations*, 148(1):9–46, 1998.
- [5] P. Biler, C. Imbert, and G. Karch. The nonlocal porous medium equation: Barenblatt profiles and other weak solutions. *Arch. Ration. Mech. Anal.*, 215(2):497–529, 2015.
- [6] I. H. Biswas, E. R. Jakobsen, and K. H. Karlsen. Difference-quadrature schemes for nonlinear degenerate parabolic integro-PDE. *SIAM J. Numer. Anal.*, 48(3):1110–1135, 2010.
- [7] J. P. Boyd. *Chebyshev and Fourier spectral methods*. Dover Publications, Inc., Mineola, NY, second edition, 2001.
- [8] A. Bueno-Orovio, D. Kay, and K. Burrage. Fourier spectral methods for fractional-in-space reaction-diffusion equations. *BIT*, 54(4):937–954, 2014.
- [9] L. Caffarelli and L. Silvestre. An extension problem related to the fractional laplacian. *Communications in partial differential equations*, 32(8):1245–1260, 2007.
- [10] ÓSCAR Ciaurri, L Roncal, PABLO RAÚL Stinga, JOSÉ L Torrea, and J. L. Varona. Fractional discrete laplacian versus discretized fractional laplacian. *arXiv preprint arXiv:1507.04986*, 2015.
- [11] S. Cifani and E. R. Jakobsen. Entropy solution theory for fractional degenerate convection-diffusion equations. *Ann. Inst. H. Poincaré Anal. Non Linéaire*, 28(3):413–441, 2011.
- [12] S. Cifani, E. R. Jakobsen, and K. H. Karlsen. The discontinuous Galerkin method for fractal conservation laws. *IMA J. Numer. Anal.*, 31(3):1090–1122, 2011.
- [13] A. Córdoba and D. Córdoba. A pointwise estimate for fractionary derivatives with applications to partial differential equations. *Proc. Natl. Acad. Sci. USA*, 100(26):15316–15317, 2003.
- [14] A. Córdoba and D. Córdoba. A maximum principle applied to quasi-geostrophic equations. *Comm. Math. Phys.*, 249(3):511–528, 2004.
- [15] F. del Teso. Finite difference method for a fractional porous medium equation. *Calcolo*, pages 1–24, 2013.
- [16] K. Diethelm, N. J. Ford, A. D. Freed, and Y. Luchko. Algorithms for the fractional calculus: a selection of numerical methods. *Comput. Methods Appl. Mech. Engrg.*, 194(6):743–773, 2005.
- [17] H. Dong, D. Du, and D. Li. Finite time singularities and global well-posedness for fractal Burgers equations. *Indiana Univ. Math. J.*, 58(2):807–821, 2009.
- [18] J. Droniou. A numerical method for fractal conservation laws. *Math. Comp.*, 79(269):95–124, 2010.

- [19] J. Droniou and E. R. Jakobsen. A uniformly converging scheme for fractal conservation laws. In *Finite Volumes for Complex Applications VII-Methods and Theoretical Aspects*, pages 237–245. Springer, 2014.
- [20] R. K. Gettoor. First passage times for symmetric stable processes in space. *Trans. Amer. Math. Soc.*, 101:75–90, 1961.
- [21] A. Gil, J. Segura, and N. M. Temme. *Numerical methods for special functions*. Society for Industrial and Applied Mathematics (SIAM), Philadelphia, PA, 2007.
- [22] R. Gorenflo, G. D. Fabritiis, and F. Mainardi. Discrete random walk models for symmetric lévy–feller diffusion processes. *Physica A: Statistical Mechanics and its Applications*, 269(1):79–89, 1999.
- [23] R. Gorenflo and F. Mainardi. Random walk models for space-fractional diffusion processes. *Fract. Calc. Appl. Anal.*, 1(2):167–191, 1998.
- [24] R. Gorenflo, F. Mainardi, D. Moretti, G. Pagnini, and P. Paradisi. Discrete random walk models for space–time fractional diffusion. *Chemical physics*, 284(1):521–541, 2002.
- [25] R. Hilfer, editor. *Applications of fractional calculus in physics*. World Scientific Publishing Co., Inc., River Edge, NJ, 2000.
- [26] Y. Huang. Explicit Barenblatt profiles for fractional porous medium equations. *Bull. Lond. Math. Soc.*, 46(4):857–869, 2014.
- [27] Y. Huang and A. Oberman. Numerical methods for the fractional Laplacian: a finite difference-quadrature approach. *SIAM Journal on Numerical Analysis*, 52(6):3056–3084, 2014.
- [28] C. Imbert and A. Mellet. Self-similar solutions for a fractional thin film equation governing hydraulic fractures. *Comm. Math. Phys.*, 340(3):1187–1229, 2015.
- [29] A. Iserles. On the numerical quadrature of highly-oscillating integrals. I. Fourier transforms. *IMA J. Numer. Anal.*, 24(3):365–391, 2004.
- [30] A. Iserles and S. P. Nørsett. On quadrature methods for highly oscillatory integrals and their implementation. *BIT*, 44(4):755–772, 2004.
- [31] N. Ju. The maximum principle and the global attractor for the dissipative 2D quasi-geostrophic equations. *Comm. Math. Phys.*, 255(1):161–181, 2005.
- [32] G. Karch, C. Miao, and X. Xu. On convergence of solutions of fractal Burgers equation toward rarefaction waves. *SIAM J. Math. Anal.*, 39(5):1536–1549, 2008.
- [33] A. Kiselev, F. Nazarov, and R. Shterenberg. Blow up and regularity for fractal Burgers equation. *Dyn. Partial Differ. Equ.*, 5(3):211–240, 2008.
- [34] M. Kwaśnicki. Ten equivalent definitions of the fractional laplace operator. *arXiv preprint arXiv:1507.07356*, 2015.

- [35] N. S. Landkof. *Foundations of modern potential theory*. Springer-Verlag, New York, 1972. Die Grundlehren der mathematischen Wissenschaften, Band 180.
- [36] S. Larsson and V. Thomée. *Partial differential equations with numerical methods*, volume 45. Springer, 2009.
- [37] J. Lund and K. L. Bowers. *Sinc methods for quadrature and differential equations*. Society for Industrial and Applied Mathematics (SIAM), Philadelphia, PA, 1992.
- [38] M. Meerschaert and C. Tadjeran. Finite difference approximations for fractional advection–dispersion flow equations. *J. Comput. Appl. Math.*, 172(1):65 – 77, 2004.
- [39] R. Metzler and J. Klafter. The random walk’s guide to anomalous diffusion: a fractional dynamics approach. *Phys. Rep.*, 339(1):77, 2000.
- [40] R. Metzler and J. Klafter. The restaurant at the end of the random walk: recent developments in the description of anomalous transport by fractional dynamics. *J. Phys. A*, 37(31):R161, 2004.
- [41] K. S. Miller and B. Ross. *An introduction to the fractional calculus and fractional differential equations*. A Wiley-Interscience Publication. John Wiley & Sons Inc., New York, 1993.
- [42] Ricardo H. Nochetto, Enrique Otárola, and Abner J. Salgado. A PDE approach to fractional diffusion in general domains: a priori error analysis. *Found. Comput. Math.*, 15(3):733–791, 2015.
- [43] K. B. Oldham and J. Spanier. *The fractional calculus: Theory and applications of differentiation and integration to arbitrary order*. Academic Press, New York-London, 1974.
- [44] I. Podlubny. *Fractional differential equations: an introduction to fractional derivatives, fractional differential equations, to methods of their solution and some of their applications*, volume 198. Access Online via Elsevier, 1998.
- [45] S. G. Samko, A. A. Kilbas, and O. I. Marichev. *Fractional integrals and derivatives: Theory and applications*. Gordon and Breach Science Publishers, Yverdon, 1993.
- [46] J. Shen, T. Tang, and L. Wang. *Spectral methods*, volume 41 of *Springer Series in Computational Mathematics*. Springer, Heidelberg, 2011. Algorithms, analysis and applications.
- [47] L. Silvestre. Regularity of the obstacle problem for a fractional power of the laplace operator. *Comm. Pure Appl. Math.*, 60(1):67–112, 2007.
- [48] E. M. Stein. *Singular integrals and differentiability properties of functions*. Princeton Mathematical Series, No. 30. Princeton University Press, Princeton, N. J., 1970.
- [49] F. Stenger. *Numerical methods based on sinc and analytic functions*, volume 20 of *Springer Series in Computational Mathematics*. Springer-Verlag, New York, 1993.

- [50] C. Tadjeran, M. M. Meerschaert, and H.-P. Scheffler. A second-order accurate numerical approximation for the fractional diffusion equation. *J. Comput. Phys.*, 213(1):205 – 213, 2006.
- [51] L. N. Trefethen. *Spectral methods in MATLAB*, volume 10 of *Software, Environments, and Tools*. Society for Industrial and Applied Mathematics (SIAM), Philadelphia, PA, 2000.
- [52] A. Truman and J.-L. Wu. Fractal Burgers’ equation driven by Lévy noise. In *Stochastic partial differential equations and applications—VII*, volume 245 of *Lect. Notes Pure Appl. Math.*, pages 295–310. Chapman & Hall/CRC, Boca Raton, FL, 2006.
- [53] E. Valdinoci. From the long jump random walk to the fractional Laplacian. *Bol. Soc. Esp. Mat. Apl. SeMA*, (49):33–44, 2009.
- [54] J. L. Vázquez. Barenblatt solutions and asymptotic behaviour for a nonlinear fractional heat equation of porous medium type. *J. Eur. Math. Soc.*, 16(4):769–803, 2014.
- [55] G. M. Zaslavsky. Chaos, fractional kinetics, and anomalous transport. *Phys. Rep.*, 371(6):461–580, 2002.
- [56] S. Zhang and J. Jin. *Computation of special functions*. A Wiley-Interscience Publication. John Wiley & Sons, Inc., New York, 1996.
- [57] A. Zoia, A. Rosso, and M. Kardar. Fractional Laplacian in bounded domains. *Phys. Rev. E*, 76:021116, Aug 2007.